Natural iron fertilization of the Atlantic sector of the Southern Ocean by continental shelf sources of the Antarctic Peninsula

Jeroen de Jong,[1,2] Véronique Schoemann,[2,3] Delphine Lannuzel,[4,5,6] Peter Croot,[7,8] Hein de Baar,[2] and Jean-Louis Tison[9]

Received 3 February 2011; revised 13 January 2012; accepted 14 January 2012; published 8 March 2012.

[1] In large parts of the Southern Ocean, primary production is limited due to shortage of iron (Fe). We measured vertical Fe profiles in the western Weddell Sea, Weddell-Scotia Confluence, and Antarctic Circumpolar Current (ACC), showing that Fe is derived from benthic Fe diffusion and sediment resuspension in areas characterized by high turbulence due to rugged bottom topography. Our data together with literature data reveal an exponential decrease of dissolved Fe (DFe) concentrations with increasing distance from the continental shelves of the Antarctic Peninsula and the western Weddell Sea. This decrease can be observed 3500 km eastward of the Antarctic Peninsula area, downstream the ACC. We estimated DFe summer fluxes into the upper mixed layer of the Atlantic sector of the Southern Ocean and found that horizontal advection dominates DFe supply, representing 54 ± 15% of the total flux, with significant vertical advection second most important at 29 ± 13%. Horizontal and vertical diffusion are weak with 1 ± 2% and 1 ± 1%, respectively. The atmospheric contribution is insignificant close to the Antarctic continent but increases to 15 ± 10% in the remotest waters (>1500 km offshore) of the ACC. Translating Southern Ocean carbon fixation by primary producers into biogenic Fe fixation shows a twofold excess of new DFe input close to the Antarctic continent and a one-third shortage in the open ocean. Fe recycling, with an estimated "*fe*" ratio of 0.59, is the likely pathway to balance new DFe supply and Fe fixation.

Citation: de Jong, J., V. Schoemann, D. Lannuzel, P. Croot, H. de Baar, and J.-L. Tison (2012), Natural iron fertilization of the Atlantic sector of the Southern Ocean by continental shelf sources of the Antarctic Peninsula, *J. Geophys. Res.*, *117*, G01029, doi:10.1029/2011JG001679.

1. Introduction

[2] Iron (Fe) plays a key role in the oceanic carbon cycle as a regulating factor of marine primary productivity [*Boyd et al.*, 2007]. The Southern Ocean is known as the largest High Nutrient Low Chlorophyll region of the global ocean [*Martin*, 1990]. Diatoms represent up to 75% of annual primary productivity in the Southern Ocean, but their growth can be limited by primarily low DFe concentrations in most of the pelagic Southern Ocean or a Fe/silicon codeficiency in Subantarctic waters north of the Polar Frontal Zone [*Hoffmann et al.*, 2008]. Light limitation and grazing pressure have also been recognized as regulating factors [*Banse*, 1996].

[3] The large-scale chlorophyll *a* (Chl *a*) distribution in the eastward flowing Antarctic Circumpolar Current (ACC) shows a bimodal pattern in the Atlantic sector of the Southern Ocean as evidenced by ocean color remote sensing (Figure 1a). One branch meandering east and downstream of the Antarctic Peninsula appears to be associated with the Southern ACC Front (SAACF) and the Polar Front (PF). A second branch stretches east of southern South America and follows the Subantarctic Front (SAF) and the Subtropical Front (STF). This suggests that Fe limitation may be alleviated along these frontal zones even a long distance away from the continental margins of South America and Antarctica. This suggests that Patagonian desert dust and/or sediments at the continental margins of southern South America and of the Antarctic Peninsula would be important

[1]Isotopes, Pétrologie, et Environnement, Département des Sciences de la Terre et de l'Environnement, Université Libre de Bruxelles, Brussels, Belgium.
[2]Department of Biological Oceanography, Royal Netherlands Institute for Sea Research, Texel, Netherlands.
[3]Laboratoire d'Ecologie des Systèmes Aquatiques, Université Libre de Bruxelles, Brussels, Belgium.
[4]Laboratoire d'Océanographie Chimique et Géochimie des Eaux, Département des Sciences de la Terre et de l'Environnement, Université Libre de Bruxelles, Brussels, Belgium.
[5]Institute for Marine and Antarctic Studies, University of Tasmania, Hobart, Tasmania, Australia.
[6]Antarctic Climate and Ecosystems Cooperative Research Centre, University of Tasmania, Hobart, Tasmania, Australia.
[7]Plymouth Marine Laboratory, Plymouth, UK.
[8]Now at Earth and Ocean Sciences, National University of Ireland, Galway, Ireland.
[9]Laboratoire de Glaciologie, Département des Sciences de la Terre et de l'Environnement, Université Libre de Bruxelles, Brussels, Belgium.

0148-0227/12/2011JG001679

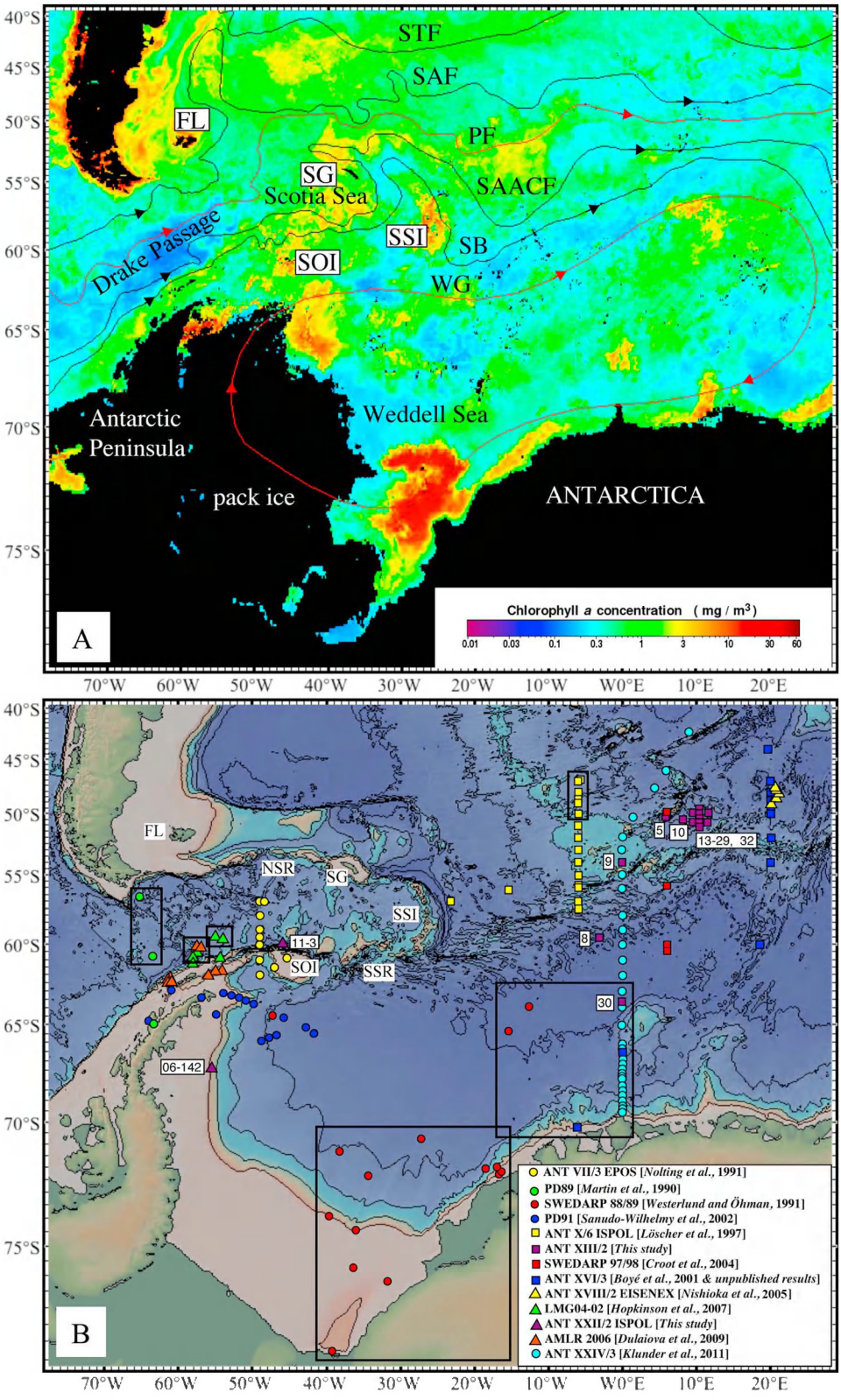
STF
SAF
PF
SAACF
SB
WG
FL
SG
Scotia Sea
SSI
SOI
Drake Passage
Antarctic Peninsula
pack ice
Weddell Sea
ANTARCTICA
Chlorophyll a concentration (mg / m3)
0.01 0.03 0.1 0.3 1 3 10 30 60
A
40°S 45°S 50°S 55°S 60°S 65°S 70°S 75°S
70°W 60°W 50°W 40°W 30°W 20°W 10°W W0°E 10°E 20°E
FL
NSR
SG
SSI
SOI
SSR
11-3
06-142
5
10
13-29, 32
9
8
30
ANT VII/3 EPOS [Nolting et al., 1991]
PD89 [Martin et al., 1990]
SWEDARP 88/89 [Westerlund and Öhman, 1991]
PD91 [Sanudo-Wilhelmy et al., 2002]
ANT X/6 ISPOL [Löscher et al., 1997]
ANT XIII/2 [This study]
SWEDARP 97/98 [Croot et al., 2004]
ANT XVI/3 [Boyé et al., 2001 & unpublished results]
ANT XVIII/2 EISENEX [Nishioka et al., 2005]
LMG04-02 [Hopkinson et al., 2007]
ANT XXII/2 ISPOL [This study]
AMLR 2006 [Dulaiova et al., 2009]
ANT XXIV/3 [Klunder et al., 2011]
B

Figure 1

potential natural Fe sources as was proposed by *de Baar et al.* [1995]. *Kahru et al.* [2007] demonstrated that ocean eddies in the ACC play an important role in cross-frontal transport of (micro)nutrients from the Antarctic Peninsula to the north, thus providing enhanced conditions for phytoplankton growth.

[4] Recently, direct and indirect evidence was found of island mass effects in the (Sub)Antarctic: the Kerguelen archipelago [*Chever et al.*, 2010; *Blain et al.*, 2008, 2007; *Bucciarelli et al.*, 2001], the Crozet Islands [*Planquette et al.*, 2007], South Georgia [*Korb et al.*, 2008, 2004] and the Antarctic Peninsula region [*Ardelan et al.*, 2010; *Dulaiova et al.*, 2009; *Korb et al.*, 2005]. Passage of the ACC across ocean ridges, along continental margins and over island shelves is thought to contribute dissolved and particulate Fe while the proximity of landmasses could also provide atmospheric dust which could partially dissolve in seawater [*Boyd and Ellwood*, 2010; *Moore and Braucher*, 2008]. Recent appreciation of continental margins as sources of dissolved and particulate Fe to the open ocean has come from field studies done by, e.g., *Severmann et al.* [2010], *Lam and Bishop* [2008], *Laës et al.* [2007], *Nédélec et al.* [2007], *Lam et al.* [2006], *Elrod et al.* [2004], and *Johnson et al.* [1999], as well as from model simulations [*Lancelot et al.*, 2009; *Moore and Braucher*, 2008].

[5] Iron is likely brought into the water column by sedimentary sources through diffusion of DFe, and resuspension of sediment particles, bringing both DFe and particulate Fe in the water column. High micromolar DFe concentrations in sediment pore water occur due the anoxic reduction and dissolution of particulate Fe phases in the sediment, which may diffuse across the sediment-water interface [*Schoemann et al.*, 1998]. This efflux depends on the organic matter load to the sediment, the remineralization rate and the oxygen penetration depth [*Sachs et al.*, 2009]. Resuspension of sediments occurs in high-energy environments. In shallow nearshore waters sediment resuspension can occur due to wind-induced wave action [*Gargett et al.*, 2004] and tidal currents [*de Jonge and van Beusekom*, 1995]. In deeper waters of the continental slope and the adjacent open ocean, sediment resuspension can occur due to tidal currents [*Bonnin et al.*, 2002], internal waves [*Hosegood et al.*, 2004], and friction between the seafloor and bottom currents [*McCave*, 1986], giving rise to nepheloid layers in waters at intermediate depth or near the seafloor.

[6] The Scotia Sea and the continental shelves of the Antarctic Peninsula region and the ocean islands around the Scotia Sea are high-energy environments [*Naveira Garabato et al.*, 2004; *Heywood et al.*, 2002], where rugged bottom topography in combination with strong internal waves and bottom currents cause high turbidity [*McCave*, 1986]. We hypothesize that in the Atlantic sector of the Southern Ocean the supply of DFe is dominated by lateral transport of DFe enriched continental shelf waters downstream of the ACC. This enrichment with DFe but also with particulate Fe is likely derived from sedimentary sources. We present here water column dissolved and particulate Fe data from two cruises with stations in the Weddell Sea, Scotia Sea and the Atlantic sector of the Southern Ocean. With these and other literature data, we will attempt to estimate the horizontal and vertical fluxes of DFe, and assess their relative importance by comparison with literature estimates of other DFe sources to the Southern Ocean such as seasonal sea ice melting, atmospheric input and iceberg calving. We will not address the role of the Argentine shelf and the possible transport of DFe from there to the ACC. While there is little data from this region [*Bowie et al.*, 2002] it is clear that due to its shallowness there is the potential for high fluxes of iron from this region [*Garcia et al.*, 2008].

2. General Hydrographic Setting

[7] The general circulation in the Southern Ocean is dominated by the ACC, which is advecting Circumpolar Deep Water (CDW) in eastward direction. Lower CDW (LCDW) is formed by mixing of North Atlantic Deep Water (NADW) with recently formed Antarctic Bottom Water (AABW) in the Atlantic sector, and is generally characterized by a salinity maximum. Upper CDW (UCDW) can be sourced in the Indian and Pacific oceans and exhibits a temperature maximum [*Naveira Garabato et al.*, 2002]. CDW becomes entrained in the northern part of the cyclonic Weddell gyre and continues as Warm Deep Water (WDW). The Weddell Sea is one of the most important locations for deep and bottom water formation. WDW is transported around the cyclonic gyre and contributes to the formation of Western Shelf Water (WSW), which as a result of atmosphere-ice-ocean interactions sinks along the Antarctic continental slope to form Weddell Sea Bottom Water (WSBW). WSBW flows to the northwest and mixes again with WDW to form Weddell Sea Deep Water (WSDW), which then leaves the Weddell Sea by spilling over the South Scotia Ridge [*Naveira Garabato et al.*, 2002; *Orsi et al.*, 1993]. WDBW is too dense to pass this sill and can only leave the Weddell Sea through gaps in the South Scotia Ridge or through the South Sandwich Trough [*Schodlok et al.*,

Figure 1. (a) Large-scale Chl *a* distribution (Aqua MODIS) in the Atlantic sector of the Southern Ocean, time averaged over the period September 2004 to March 2005. Chlorophyll *a* image courtesy NASA (level 3 ocean color products available from http://oceancolor.gsfc.nasa.gov/). Hydrographic fronts are indicated by black or red (Polar Front) arrowed lines with the arrows indicating flow direction. Hydrography after *Orsi et al.* [1995]: PF, Antarctic Polar Front; SAACF, Southern Antarctic Circumpolar Current Front; SAF, Subantarctic Front; SB, Southern Boundary Antarctic Circumpolar Current Front; STF, Subtropical Front; WG, Weddell Gyre. (b) Stations of Fe biogeochemistry expeditions treated in section 5.2 (see also Table S1) superimposed on Southern Ocean bathymetry (NASA-ASTER-USGS Elevation Model [*Ryan et al.*, 2009]). Isobaths are at 1000 m intervals. Note that the stations inside the rectangles have not been used for DFe flux calculations (see section 5.2 and Figure 6). The stations representing new Fe data from this study are indicated in purple triangles (ANT XXII/2 ISPOL) and purple squares (ANT XIII/2), with their station numbers indicated. Geographic locations: FL, Falkland Islands; NSR, North Scotia Ridge; SG, South Georgia; SOI, South Orkney Islands; SSI, South Sandwich Islands; SSR, South Scotia Ridge.

2002]. The pathways of the water masses leaving the Weddell Sea are strongly influenced by the rugged bottom topography of the South Scotia Ridge with its shelves, basins and troughs [*von Gyldenfeldt et al.*, 2002; *Heywood et al.*, 2002]. WDW and WSDW mix with waters from the Bransfield Strait and the ACC in the Weddell Scotia Confluence (WSC), but the water masses also undergo local modification due to the influence of shelf waters from the northwestern Weddell Sea [*Whitworth et al.*, 1994; *Patterson and Sievert*, 1980].

3. Material and Methods

[8] Our sampling and analytical procedures are described in detail by *de Jong et al.* [1998, 2008] but are briefly summarized in this section.

3.1. Sampling and Analytical Procedures

3.1.1. ANT/XIII-2: DFe-0.4 μm

[9] During cruise ANT/XIII-2 of RV *Polarstern* between 4 December 1995 and 24 January 1996 in the Atlantic sector of the Southern Ocean, ten water column profiles were sampled at ten depths down to 500 m depth within a small patch of the Polar Frontal Zone (PFZ) at ~50°S, 10°E, as well as five more profiles in the southern Antarctic Circumpolar Current (ACC) and the Weddell Sea along a transect in southerly direction between 50°S, 10°E and 64°S, 0°E (Figure 1b and Table S1 in the auxiliary material).[1] General Oceanics (Miami, FL, USA) GoFlo bottles of 11 L were deployed from a Kevlar hydrowire and tripped with Teflon polytetrafluoroethylene (PTFE) messengers. Upon return to the deck, the samplers were mounted in storage cabinets outside a clean air van and connected to the interior using Teflon perfluoroalkoxy (PFA) tubing. The GoFlo bottles were nitrogen-pressurized in line to 0.5 bar and the seawater was filtered through acid-cleaned polycarbonate membrane filters (Poretics, pore size 0.4 μm, diameter 47 mm) inside Teflon PTFE filter holders. The filtered seawater was collected in 250 mL low-density polyethylene (LDPE) bottles for measurement of DFe. Before acidifying, the samples were left in the dark for 1 h to reoxidize any present Fe(II) to Fe(III) in the absence of photoreduction. The samples were then acidified to pH 1.9 with 250 μL subboiled concentrated HNO_3 to 250 mL of sample.

[10] Analysis was done within 24 h with a shipboard flow injection analyzer (Fe-FIA-CL), which preconcentrates Fe (III) on a column of TSK-8HQ resin [*Landing et al.*, 1986]. The acidified seawater sample was buffered in line by addition of clean ammonium acetate buffer to obtain an optimal chelating pH of ~4.0. The detection is based on the chemiluminescence produced by the iron-mediated oxidation of luminol by hydrogen peroxide [*Obata et al.*, 1993]. Calibrations were done by standard additions to acidified low-Fe Antarctic seawater. We found total blanks and detection limits (3x SD of blank) of 0.022 ± 0.007 nmol/L (n = 10) and 0.021 nmol/L, respectively. Precision (1SD) was typically around 2%–5% across the working range of concentrations at the 0.05–2 nmol/L level. The accuracy of the Fe-FIA-CL system was verified by analyzing NASS-4 reference seawater from the National Research Council of Canada. The results were in good agreement with the certified values: Fe 1.88 ± 0.15 nmol/L (n = 9), NASS-4 certified 1.88 ± 0.29 nmol/L.

3.1.2. ANT/XXII-2 ISPOL: DFe-0.2 μm, TD-Fe, and REF-Fe Measurements

[11] During Ice Station Polarstern (ISPOL), cruise ANT/XXII-2 between 27 November 2004 and 2 January 2005, two water column profiles were sampled (Figure 1b and Table 1) down to the seafloor. Station 06-142 was situated in the western Weddell Sea on the continental slope of the Antarctic Peninsula down to1386 m, while station 011-3 was located in the Weddell Scotia Confluence 70 km north of Coronation Island of the South Orkneys in 4283 m deep waters between the South Orkney Plateau and Pirie Bank. Water samples were taken using 10 L General Oceanics Niskin samplers, on an epoxy-coated rosette frame with a Sea-Bird 911+ CTD. Niskin bottles have been used before to provide reliable Fe data [*Measures and Vink*, 2001]. Upon recovery on deck, subsamples were immediately taken from each Niskin in 250 mL LDPE bottles for measurement of TD-Fe (total dissolvable Fe, unfiltered) and DFe. In a clean air van equipped with class 100 laminar flow hoods, samples for DFe were filtered using polycarbonate filtration devices (Sartorius) with polycarbonate membrane filters (Nuclepore, 0.2 μm pore size, 47 mm diameter). Gentle vacuum (<0.5 bar) was applied with a Masterflex hand pump. The samples were acidified to pH 1.9 with 250 μL concentrated subboiled HNO_3 to 250 mL of sample.

[12] TD-Fe and DFe were analyzed 3 years after sample collection and acidification by a recently developed isotope dilution technique [*de Jong et al.*, 2008]. Sample preparation consisted of a preconcentration step by microcolumns filled with the resin NTA Superflow (Qiagen, Netherlands). NTA Superflow quantitatively extracts Fe from seawater samples at a pH as low as 1.7 [*Lohan et al.*, 2005]. Seawater samples (50 mL) were spiked with ^{54}Fe and after an equilibration/reaction time of 15 min allowed to pass by gravity through the NTA microcolumns. The columns were then rinsed with acidified UHP to rinse off remaining sea salts and the Fe was eluted with 1 M HNO_3 into Savillex PFA screw cap beakers. The samples were dried down on a hotplate at 125°C inside a clean air fume cabinet. Prior to analyses the samples were redissolved in 500 μL 0.05 M HNO_3 yielding a preconcentration factor of 100. Isotope dilution measurements were done using a Nu Plasma multicollector ICP-MS (Nu Instruments, Wrexham, UK) in dry plasma mode through the use of an Aridus II desolvating sample inlet system (Cetac Technologies, Omaha, NE, USA). Concentrations based on the $^{57}Fe/^{54}Fe$ ratio measurement are reported, while the $^{56}Fe/^{54}Fe$ ratio measurement served to check internal consistency of the results. Blanks were low and reproducible (0.045 ± 0.020 nmol/L, n = 21, 3 × SD detection limit per session 0.020–0.069 nmol/L range) and precisions were typically 1%–2% [*de Jong et al.*, 2008].

[13] For quality control purposes we regularly analyzed Sampling and Analysis of Fe (SAFe) reference seawater [*Johnson et al.*, 2007] that have the following assigned consensus values: Surface-1 (0.097 ± 0.043 nmol/L) and Deep-2 (0.91 ± 0.17 nmol/L). Our grand mean values for Surface-1 (0.089 ± 0.021 nmol/L, 1SD, n = 13) and Deep-2 (0.939 ± 0.047 nmol/L, 1SD, n = 18) are in good agreement with these assigned consensus values.

[1] Auxiliary materials are available in the HTML. doi:10.1029/2011JG001679.

Table 1. Water Column Fe Concentrations at ANT XXII/2 ISPOL by ID-MS[a]

Depth (m)	DFe (nmol/L)	TD-Fe (nmol/L)	REF-Fe (nmol/L)	PL-Fe (nmol/L)	PFe (nmol/L)	T-Fe (nmol/L)
Station 06-142, 1 January 2005 (67°22'S, 55°25'W, Seafloor 1386 m)						
−1	0.58	NA	NA	-	-	-
−20	0.56	3.10	5.18	2.54	7.72	8.28
−50	0.89	1.64	5.46	0.75	6.21	7.10
−100	0.80	1.82	4.69	1.03	5.72	6.52
−200	0.88	1.75	4.00	0.87	4.87	5.74
−300	1.17	3.65	4.30	2.48	6.78	7.95
−500	1.88	3.62	5.80	1.74	7.54	9.42
−700	2.03	5.52	4.23	3.49	7.72	9.75
−1000	2.78	8.40	7.03	5.63	12.66	15.44
−1200	5.55	11.02	2.03	5.47	7.50	13.04
−1300	11.50	23.44	2.86	11.94	14.80	26.30
−1340	22.68	42.17	2.54	19.49	22.03	44.71
−1376	20.40	60.68	4.65	40.28	44.92	65.33
Station 011-3, 7 January 2005 (59°55'S, 45°55'W, Seafloor 4283 m)						
−20	3.63	5.51	0.90	1.88	2.78	6.41
−40	2.75	3.10	0.52	0.35	0.87	3.63
−60	3.37	4.10	0.51	0.73	1.23	4.60
−80	7.83	8.07	0.29	0.24	0.53	8.36
−100	12.83	13.22	0.36	0.39	0.75	13.57
−150	10.85	11.30	NA	0.45	-	-
−200	12.09	14.01	NA	1.91	-	-
−300	12.08	15.29	0.68	3.21	3.89	15.98
−400	10.14	11.03	0.93	0.88	1.81	11.96
−500	12.05	12.78	0.46	0.72	1.19	13.24
−750	7.91	9.78	0.34	1.87	2.21	10.12
−1000	2.94	6.24	0.22	3.31	3.53	6.46
−1250	2.20	8.28	0.62	6.08	6.69	8.89
−1500	4.07	9.44	0.36	5.37	5.73	9.80
−1750	3.29	5.88	0.89	2.59	3.48	6.76
−2000	3.49	6.38	0.13	2.89	3.02	6.50
−2500	3.86	6.68	0.24	2.82	3.06	6.92
−3000	4.21	12.61	0.52	8.40	8.92	13.13
−3500	8.33	33.51	0.84	25.18	26.02	34.35
−4000	8.76	49.48	1.01	40.72	41.73	50.49
−4100	11.55	45.22	1.77	33.67	35.43	46.99
−4200	14.61	53.93	2.54	39.32	41.86	56.47
−4270	10.10	55.35	1.83	45.25	47.08	57.18

[a]NA, not analyzed.

[14] TD-Fe represents the sum of DFe and a dilute nitric acid (0.014 M, pH 1.9) dissolvable portion of the particulate Fe, with some refractory Fe possibly escaping dissolution and detection. To obtain total Fe concentrations, the refractory particulate Fe (REF-Fe) concentrations should be measured also. This was determined by filtering between 70 and 180 mL of the unfiltered acidified seawater samples using a polycarbonate filtration device (Sartorius) with polycarbonate membrane filters (Nuclepore, 0.2 μm pore size, 47 mm diameter). The filters were rinsed off with UHP water in the filtration apparatus to remove sea salts, and directly transferred into Savillex PFA screw cap beakers to which a mixture of $HNO_3/H_2O_2/HF$ (2000/500/250 μL) was added as well as a ^{54}Fe spike. Care was taken to wet all parts of the filter. The samples were left for 4 hours at room temperature. They were ultrasonicated during 15 min to better solubilize/suspend the particles. The filters were then removed from the Savillex beakers with polypropylene tweezers, to prevent that polycarbonate filter debris formed during the hot acid digestion interferes with further sample manipulations. The filters were rinsed off above the beakers with UHP water and the samples heated during 24 h to 125°C on a hot plate inside a clean air fume hood, dried down to drive off fluorides and chlorides, redigested with 100 μL subboiled 14 M HNO_3, dried down again and redissolved in 500 μL 0.05 M HNO_3 for MC-ICP-MS measurement. Filter blanks amounted to 6.0 ± 0.9 ng Fe (1SD, n = 4). To test the efficiency of the acid digestion method and to verify if these nonpurified samples exhibited any significant isobaric (poly atomic) interferences, the reference materials IAEA-392 (green algae) and IAEA-405 (estuarine sediment) from the International Atomic Energy Agency were analyzed. Possible interfering species are $^{40}Ca^{16}O^{1}H$, $^{40}Ca^{16}O$, ^{54}Cr, $^{37}Cl^{16}O^{1}H$, $^{37}Cl^{16}O$ and $^{40}Ar^{13}C$ (interferes with Cr correction on mass 54 using ^{53}Cr). For IAEA-392 we found 504 ± 3 μg/g with the $^{57}Fe/^{54}Fe$ ratio and 498 ± 3 μg/g with the $^{56}Fe/^{54}Fe$ ratio (2SD, n = 2). For IAEA-405 this was 3.80 ± 0.08% ($^{57}Fe/^{54}Fe$) and 3.80 ± 0.07% ($^{56}Fe/^{54}Fe$) (2SD, n = 2). The excellent agreement with the certified values (IAEA-392: 497 ± 13 μg/g; IAEA-405: 3.74 ± 0.07%), demonstrates the fitness for purpose of this technique for biological and lithogenic sample types.

[15] In the following we will present the Fe data as the measured parameters TD-Fe, DFe and REF-Fe, as well as the derived parameters Total Fe (T-Fe = TD-Fe + REF-Fe) and Particulate Labile Fe (PL-Fe = TD-Fe – DFe). It should be noted that PL-Fe is a highly operationally defined parameter, which depends on the strength and type of acid,

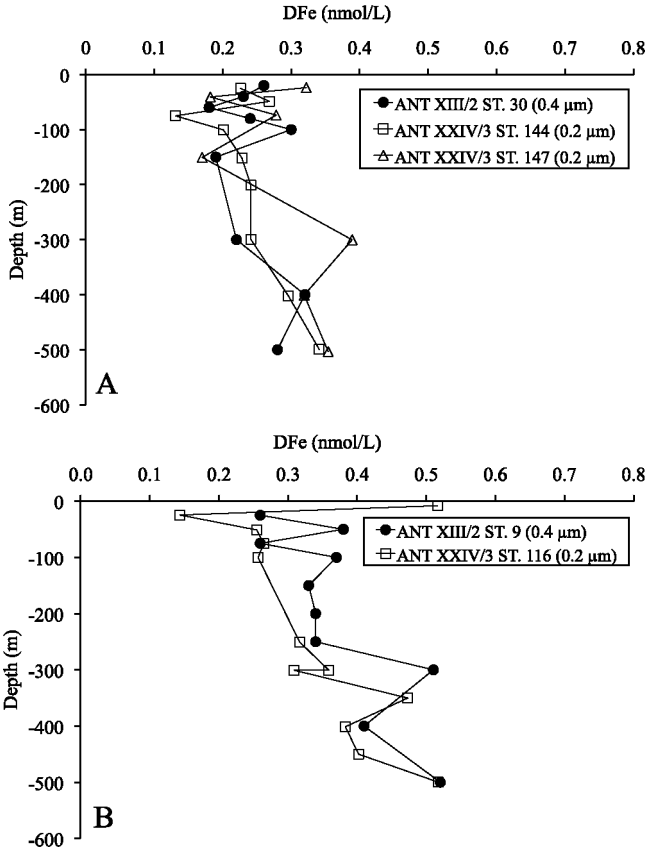

Figure 2. Compatibility of DFe-0.4 μm and DFe-0.2 μm data. (a) Vertical profiles of DFe-0.4 μm at ANT XIII/2 station 30 (63°40′S, 0°00′E) (this study) and DFe-0.2 μm at ANT XXIV/3 stations 144 (63°00′S, 0°00′E) and 147 (63° 58′S, 0°00′E) [*Klunder et al.*, 2011]. (B) Vertical profiles of DFe-0.4 μm at ANT XIII/2 station 9 (54°00′S, 0°00′E) (this study) and DFe-0.2 μm ANT XXIV/3 station 116 (54°00′S, 0°00′E) [*Klunder et al.*, 2011].

the length of time and temperature of storage, and the type of particles in the unfiltered sample [*Berger et al.*, 2008]. It is likely that this parameter overestimates the potentially bioavailable portion of the particulate matter [*Berger et al.*, 2008], which is beyond the scope of this paper. It serves here to illustrate trends in labile and refractory Fe. DFe represents a size cutoff of 0.2 μm (ANT XXII/2 ISPOL) or 0.4 μm (ANT XIII/2) and may contain apart from free ionic Fe also (in)organic colloidal Fe, nanoparticulate Fe as well as truly soluble (in)organic Fe complexes.

3.1.3. Compatibility of 0.2 μm and 0.4 μm Filtered DFe Data

[16] We could demonstrate that 0.4 μm and 0.2 μm DFe data are probably compatible, by comparing vertical profiles of DFe filtered over 0.4 μm and 0.2 μm from two different cruises but at same or similar positions and both measured with the same analytical technique (Fe-FIA-CL). A vertical profile of DFe-0.4 μm at ANT XIII/2 station 30 (this study) at 63°40′S, 0°00′E showed a similar profile as DFe-0.2 μm ANT XXIV/3 stations 144 (63°00′S, 0°00′E) and 147 (63° 58′S, 0°00′E) (Figure 2a) [*Klunder et al.*, 2011]. DFe-0.4 μm at ANT XIII/2 station 9 (this study) at 54°00′S, 0°00′E was slightly higher than DFe-0.2 μm ANT XXIV/3 station 116 (54°00′S, 0°00′E) (Figure 2b) [*Klunder et al.*, 2011]. This may have been due to a pore size effect, but could also reflect natural variability as the samples were collected 12 years apart, and may be subject to variability in the flow field or mixing characteristics. However, as we present data as average concentrations in the upper 200 m, we deem the relatively small difference between DFe filtered across 0.2 μm and 0.4 μm as not significant (see Table S1).

4. Results

4.1. Hydrographic Stratification

[17] The water masses that were encountered in the western Weddell Sea (station ANT XXII/2 06-142) were cold Winter Water (WW) of −1.84°C in the upper 200 m, with a relatively fresh surface stratified layer of 30 m thick with salinity 34.19. Warmer (0.56°C) and saltier (34.67) WDW was present with its core around 600 m, with below 1000 m WSDW and near the seafloor cold (−1.61°C), dense WSBW (Figure 3a).

[18] In the Weddell Scotia Confluence (station ANT XXII/2 011-3) we found a surface stratified layer of 40 m atop Antarctic Surface Water (AASW) in the upper 150 m. The hydrographical stratification became rather chaotic until 750 m because of vigorous mixing of WDW with CDW of the Scotia Sea, causing an interleaving of layers (Figure 3c). The core of CDW can be found at 1200 m. Below the 0°C isotherm at 1900 m, WSDW can be found until the seafloor (Figure 3c).

4.2. ANT XXII/2 ISPOL: Iron in the Western Weddell Sea

[19] The vertical profiles of T-Fe, TD-Fe and DFe at station 06-142 are shown in Figure 4a whereas PL-Fe and REF-Fe profiles are displayed in Figure 4b. Concentration data are listed in Table 1. Concentrations of DFe are ~0.6 nmol/L in the surface mixed layer (30 m), ~0.9 nmol/L right below the mixed layer and throughout the thermocline until 200 m, then tend to increase to 2–3 nmol/L between 500 and 1000 m. Below 1200 m DFe is strongly enhanced to a maximum of ~20 nmol/L near the seafloor at 1386 m. TD-Fe follows the same trend with concentrations higher than DFe by a factor of 2–3, except TD-Fe at 20 m which is 5 times higher than DFe. Total dissolvable Fe reaches a maximum of 60 nmol/L near the seafloor. Similarly shaped vertical TD-Fe profiles with 1–2 nmol/L in the upper water column until ~25 nmol/L in the bottom water, have been reported on the continental shelf of the southeast and southern Weddell Sea [*Westerlund and Öhman*, 1991]. PL-Fe exhibits concentrations of around 1 nmol/L in the upper 200 m. There is however a peak of 2.5 nmol/L in the Chl *a* maximum at 20 m. Between 300 and 1200 m there is a gradual increase of PL-Fe to 5 nmol/L and below 1200 m PL-Fe rapidly increases until 40 nmol/L. Significant concentrations of REF-Fe are present across the water column: a rather constant 5 ± 1 nmol/L in the upper 1000 m, but drop to 3 ± 1 nmol/L below 1200 m until just above the seafloor at 1376 m.

4.3. ANT XXII/2 ISPOL: Iron in the Scotia Sea

[20] Despite being a deep ocean station, the DFe concentrations at station 011-3 (Table 1 and Figure 4d) are remarkably enhanced with levels between 3 and 5 nmol/L in

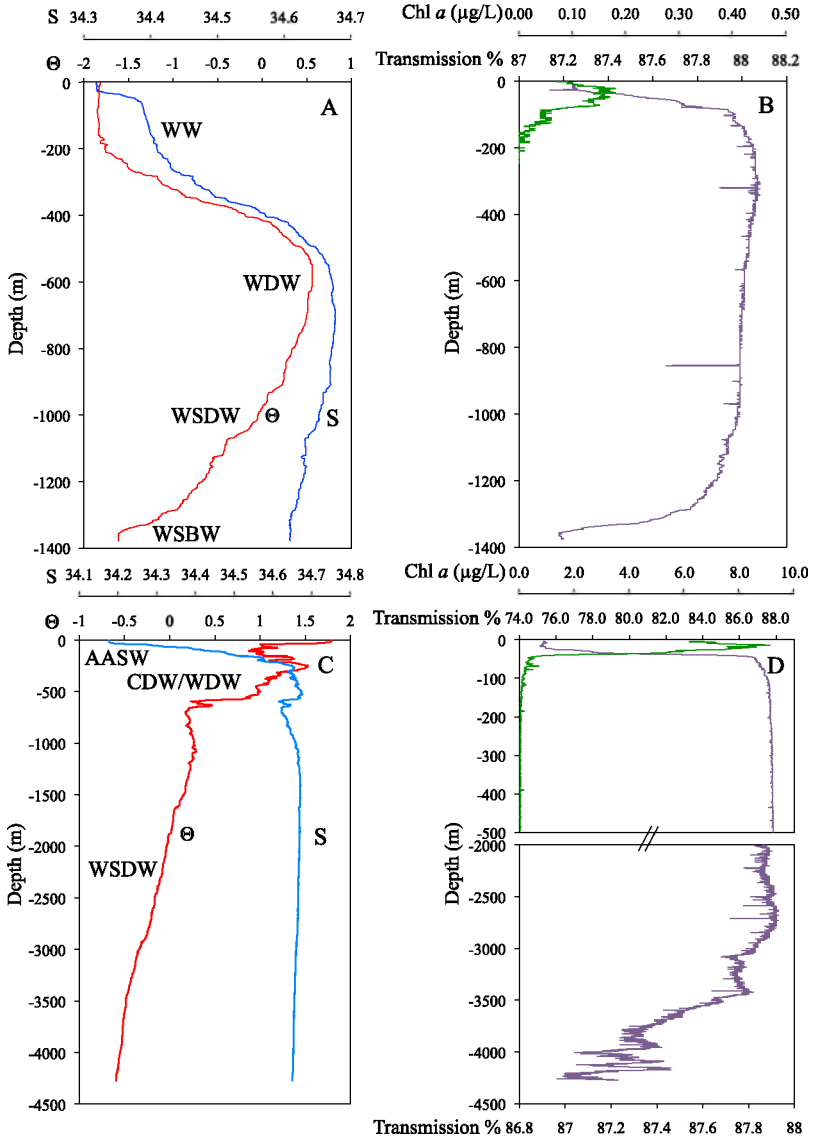

Figure 3. ANT XXII/2 ISPOL CTD profiles at (a, b) station 06-142 (Weddell Sea) and (c, d) station 011-3 (Weddell-Scotia Sea Confluence) [*Absy et al.*, 2008]. Represented are potential temperature Θ (red line), salinity S (blue line), light transmission (purple line), and Chl *a* (µg/L) (green line). Water masses are Winter Water (WW), Warm Deep Water (WDW), Weddell Sea Deep Water (WSDW), Weddell Sea Bottom Water (WSBW), Antarctic Surface Water (AASW), and Circumpolar Deep Water (CDW).

the upper 60 m, increasing to 13 nmol/L between 100 and 500 m, then lower at 2–4 nmol/L between 1000 and 3000 m, followed by an increase toward the seafloor to 10–14 nmol/L. Interestingly, TD-Fe is just slightly higher than DFe in the upper 750 m, resulting in low PL-Fe values of ~0.5 nmol/L, except for a peak at 20 m of 1.9 nmol/L in the Chl *a* maximum and at 200–300 m, where PL-Fe reaches ~3 nmol/L. A third PL-Fe maximum is located at 1250 m depth with concentrations up to ~6 nmol/L. Until 2500 m PL-Fe stays around 2.5–3 nmol/L, but below 2500 m until the bottom PL-Fe increases strongly to reach a maximum of 45 nmol/L near the seafloor. REF-Fe is much lower throughout the water column than at the Weddell Sea station: 0.5 ± 0.2 nmol/L until 1750 m, followed by a gradual increase from a minimum at 2000 m of 0.13 nmol/L to 2–2.5 nmol/L near the seafloor.

4.4. ANT XIII/2: Iron in the Upper 500 m of the ACC Between 60°S, 3°W and 50°S, 10°E

[21] Dissolved Fe concentrations (data available in Table S1) as measured in the upper 500 m of a small area in the PFZ at positions ranging between 49°30′S–50°42′S and 9°33′E–11°32′E show typical nutrient type profiles and are uniformly low (0.1–0.3 nmol/L) (Figure 5). The profiles exhibit surface enrichment in the upper 50 m from 0.1 nmol/L toward 0.26 nmol/L, a subsurface minimum of 0.05–0.1 nmol/L between 75 and 150 m followed by a gradual increase to 0.3 nmol/L at 500 m. Outside this area, going from the PFZ to the southwest and closing in on the Antarctic continent, via the stations 9, 5 and 10 into the southern ACC until station 8 in the Marginal Ice Zone (MIZ), a gradual increase of DFe

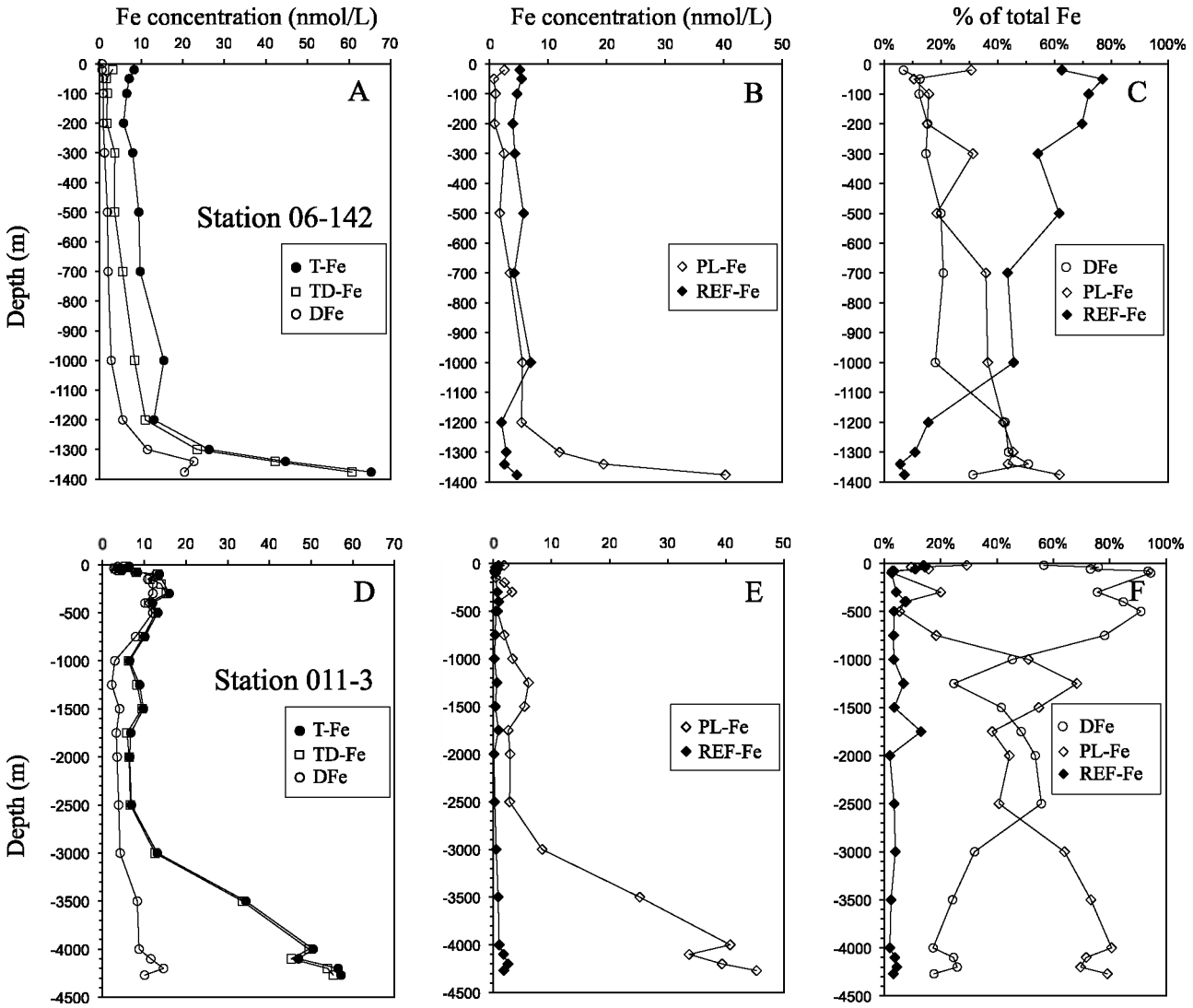

Figure 4. Profiles of DFe, TD-Fe, T-Fe, REF-Fe, and PL-Fe concentrations at (a, b) stations 06-142 (Weddell Sea) and (d, e) station 011-3 (Weddell-Scotia Sea Confluence) during ISPOL ANT XXII/2. (c, f) Percentage contributions of DFe, PL-Fe, and REF-Fe to T-Fe at these two stations are displayed, respectively.

can be discerned (Figure 5) to 0.2–0.5 nmol/L in the upper 100 m and 0.6–0.7 nmol/L at depth.

5. Discussion

5.1. Iron Profiles During ANT XXII/2 ISPOL

[22] At the Weddell Sea station 06-142, the relatively fresh stratified layer may indicate recent sea ice spring melting. Sea ice cores taken at this station during the ISPOL time series study showed interstitial brine salinities that as a result of spring melting had become fresher than the underlying seawater [*Lannuzel et al.*, 2008]. No large icebergs as sources of fresh water were observed near the station.

[23] The concentrations of DFe (0.58 nmol/L) and PL-Fe (2.54 nmol/L) in the upper mixed layer are comparable to the East Antarctic study by *van der Merwe et al.* [2011], who found in seawater under the pack ice mean values of 0.70 nmol/L DFe and 2.97 nmol/L PL-Fe. The only

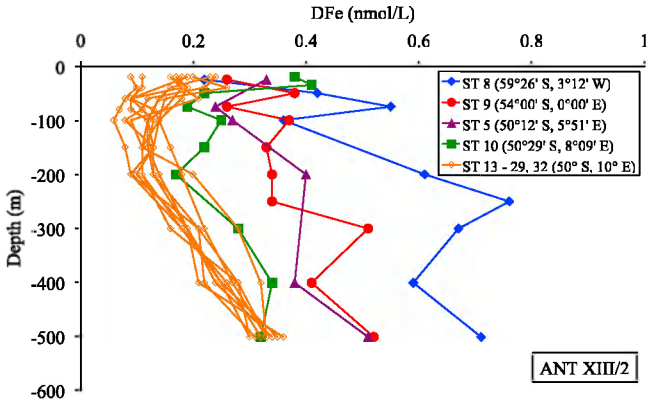

Figure 5. Eastward decrease of DFe as seen in the vertical profiles of DFe in the upper 500 m of the Antarctic Circumpolar Current, during cruise ANT XIII/2.

exception is the higher contribution of REF-Fe in our study. Below the upper mixed layer of 33 m REF-Fe remains high, but PL-Fe decreases strongly to 0.9 nmol/L and DFe increases to 0.9 nmol/L.

[24] The low DFe versus high particulate Fe at 20 m depth could be explained in terms of decoupling of DFe and particulate Fe release from melting sea ice [*van der Merwe et al.*, 2011]. Particulate Fe in sea ice is mostly associated with the ice and less so with the brine [*van der Merwe et al.*, 2011]. During the ISPOL time series study, an initial phase of brine drainage advected DFe to the under-ice seawater. This was followed by freshening of the sea ice brine, as the sea ice continued melting. Most of the DFe was released during the first 10 days of the ISPOL time series study [*Lannuzel et al.*, 2008]. The freshening of the brines resulted in a less strong density gradient with the underlying seawater resulting in a strong decrease of brine drainage of DFe. Indeed, after this period the DFe in the under-ice seawater as sampled in situ, was seen to decrease [*Lannuzel et al.*, 2008]. TD-Fe showed a concomitant increase as continued melting of the sea ice resulted in the release of particulate matter from the ice. Toward the end of the ISPOL time series a considerable ice cover was still present but had the appearance of rotten ice, due to strongly increased porosity.

[25] The possibility of particulate matter being released by the melting sea ice and the observations of Chl *a* concentrations of ~0.5 μg/L and a surface minimum in beam transmission (Figures 3b and 4c) could signify seeding of sea ice algae in the upper water column.

[26] Below the stratified layer of 33 m, the percentage REF-Fe is high at 80% of T-Fe, but gradually decreases until less than 10% near the seafloor. At the same time the percentages of DFe and PL-Fe increase with depth, but stronger so for DFe below 1200 m. These high DFe and PL-Fe values near the seafloor indicate a sediment source of DFe in bottom waters, either from diffusion across the sediment water interface of high DFe in reducing pore waters or by infusion of these pore waters by sediment resuspension [*Latimer and Filippelli*, 2007; *Pakhomova et al.*, 2007; *Elrod et al.*, 2004]. The beam attenuation profile (Figure 3b) indicated the presence of a nepheloid layer in the lowermost 250 m, which implies that sediment resuspension is the likely mechanism for bringing DFe into near-bottom waters. Most of the diagenetic DFe would rapidly reoxidize at or beyond the sediment-water interface and precipitate as Fe oxyhydroxide nanoparticles. At this point these Fe nanoparticles may still pass through a 0.2 μm membrane filter and be detectable as DFe. Further aggregation into colloidal material and adsorption to suspended particles, such as in the form of coatings on aluminosilicates (clay minerals), causes the DFe to pass into the PL-Fe phase. Indication of the freshly formed nature of the particulate Fe below 1200 m comes from the near absence of REF-Fe below 1200 m, as well as a higher percentage PL-Fe and a drop in the concentration and percentage of DFe just above the seafloor due to particle adsorption of DFe.

[27] The presence of appreciable amounts of REF-Fe in the upper 1000 m may be indicative of insoluble aged Fe bearing mineral particles and/or lithogenic particles in the water column of the Weddell Sea. The Weddell Gyre, while flowing along the southeastern continental margin of the Weddell Sea, is likely picking up DFe from sediment sources, which may initially be present as freshly precipitated ferrihydrite in the PL-Fe fraction. It is then transported clockwise to the north along the western continental margin (Figures 1a and 1b). During this transport, PL-Fe may become more refractory due to the aging of these Fe bearing minerals and become REF-Fe. Lithogenic particles might be present as well, derived either from lateral transport of suspended particles from shallow waters of the inner continental shelf or from release of ice rafted sediment and aerosol particles from melting sea ice and icebergs [*Raiswell et al.*, 2008]. This may explain the high percentage of REF-Fe in the upper 200 m of 70%–80% in coincidence with reduced transmission in the beam attenuation profile (Figure 3b). To this we could add our visual observation of dirty sea ice (grit, pebbles, small boulders) in the Powell Basin and the Philip Passage between the Antarctic Peninsula and the South Orkneys.

[28] At station 011-3 (Weddell Sea/Scotia Sea Confluence, in the South Orkney Trough near Pirie Bank), DFe exhibits a broad maximum in the upper 500 m of ~12 nmol/L with the percentage DFe reaching values higher than 90% of T-Fe and PL-Fe just a few percent. In the surface mixed layer of 38 m, DFe at 20 m is lower at 3.6 nmol/L, which is 57% of T-Fe, while PL-Fe is higher at 29% (Figure 4f). A pronounced minimum in the beam attenuation, together with a high Chl *a* concentration of 9 μg/L, point at blooming conditions of phytoplankton and biological uptake of DFe (Figure 3d). REF-Fe reaches here also its highest relative contribution of about 14% of T-Fe, which may be a result of release of sea ice rafted lithogenic material or refractory Fe associated to diatom frustules. The depth range over which the DFe is at maximum, with a small PL-Fe peak at 200–300 m suggests that DFe and particulate Fe were derived from the shallow waters over the South Orkney Plateau (Figure 1b). The observation that in the upper 500 m up to 94% of the Fe is in the dissolved size class (<0.2 μm) suggests that these waters have been in recent contact with sediment sources, and that this DFe is still in its nanoparticulate or colloidal form before aggregating to form particles >0.2 μm. It is possible that organic ligands of benthic origin assist in maintaining Fe in the dissolved phase [*Gerringa et al.*, 2008].

[29] The increases of all Fe concentrations around 1250–1500 m, with PL-Fe reaching a maximum to comprise 68% of T-Fe at 1250 m depth (Figures 4d–4f), may be an indication that these waters have been in contact with a continental margin also, but maybe less recently, so that the DFe has had more time to be transferred to the PL-Fe fraction. Over the same depth range, REF-Fe concentrations are also somewhat enhanced and peak at 1750 m with a relative contribution of 13% of T-Fe. The depth at which this maximum occurs seems to coincide with the general sill depth of the South Scotia Ridge (Figure 1b).

[30] Below 2500 m, DFe, REF-Fe and particularly PL-Fe increase steadily toward the seafloor in the deeper part of the South Orkney Trough, concomitant with a steady decrease of the beam transmission signal (Figures 3d and 4d). High PL-Fe up to 45 nmol/L in these deep waters is an indication of the considerable contact these waters have had with continental margins. These waters, mainly WSDW, have been flowing along and across the eastern continental slope of the Antarctic Peninsula, picking up DFe and particulate

Fe by sediment resuspension and benthic diffusion such as at our station 06-142, before being deflected eastward along the south-facing slope of the South Scotia ridge. Then, through gaps in the ridge such as the Philip Passage and Orkney Passage, respectively west and east of the South Orkney Islands (Figure 1b), the WSDW spills down into the South Orkney Trough while turning in westward direction into the Drake Passage [*Heywood et al.*, 2002; *Schodlok et al.*, 2002]. Lateral transport of fine particulate Fe at depth, may also constitute a source of Fe to the upper mixed layer by upwelling and deep winter mixing. Part of PL-Fe may be directly accessible to phytoplankton [*Nodwell and Price*, 2001], but may also be rendered bioavailable through solubilization by photoreduction, organic complexation, reducing microenvironments in organic aggregates and zooplankton grazing [*Lam and Bishop*, 2008; *Lam et al.*, 2006].

5.2. Lateral Decrease of DFe in the ACC Downstream of the Antarctic Peninsula

[31] The decreasing DFe concentrations with increasing distance from the continental shelves of the Antarctic Peninsula and the islands in between, as was observed at ANT XIII/2, suggests that these landmasses may provide DFe that is transported by horizontal diffusion/advection as far east as the stations occupied during this cruise. To further corroborate this, we combined our DFe data with published DFe data from cruises that took place in the western Weddell Sea, the Peninsula area and the Atlantic sector of the Southern Ocean (Table S1). The decrease of DFe averaged over the upper 200 m (Table 2 and Table S1) with increasing distance from the Antarctic coastline is illustrated in Figure 6. The upper 200 m was chosen, as it comprises the mixed layer depths during deep winter mixing, and also integrates Fe uptake by phytoplankton and much of its subsequent release at depth by remineralization as to minimize underestimations of the DFe inventory due to biological uptake. At those stations where only one surface or near-surface concentration is given for the upper 200 m [e.g., *Sañudo-Wilhelmy et al.*, 2002], this value is taken as the average for the upper 200 m. Figure 6 shows for the western Weddell Sea and the ACC nonlinearly decreasing DFe concentrations with increasing distance from the nearest Antarctic coastline. The distances were determined using GeoMapApp online software provided by the Marine Geoscience Data System (www.marine-geo.org) [*Carbotte et al.*, 2007]. The DFe decrease eastward of the Antarctic Peninsula and the South Sandwich Islands can be observed as far as 3500 km away (Figure 6).

5.2.1. Excluded Data

[32] The following stations were excluded because their DFe concentrations belonged to different hydrographic/geochemical regimes than that of the Peninsula area leading them to lie above or below the eastward decreasing trend of DFe (Figure 6):

1. PD89 stations 1 and 2 from *Martin et al.* [1990], LMG04-02 stations 27 (A1/A3), 42 (M1), 55 (A2/A4), and 64 (M2/M3) from *Hopkinson et al.* [2007] and AMLR 2006 stations 08-02 and 09-02 from *Dulaiova et al.* [2009]. These off-shelf stations comprised predominantly upstream DFe depleted ACC waters [*Hopkinson et al.*, 2007] derived from the Pacific Southern Ocean [*de Baar et al.*, 1999].

2. Stations in the southeastern Weddell Sea, namely all SWEDARP88/89 stations, except station 43 close to the Antarctic Peninsula [*Westerlund and Öhman*, 1991]. Although these stations exhibit DFe enrichment in nearshore waters, they belong to a different hydrographic regime, namely the southeastern flank of the Weddell Gyre.

3. ANT XIII/2 station 30 (this study), ANT XVI/3 stations 182 and 185 [*Boyé et al.*, 2001], and ANT XXIV/3 stations 144–178 and surface samples [*Klunder et al.*, 2011]. These stations are further east than those of *Westerlund and Öhman* [1991], and despite their proximity to the continental shelf, their DFe here remains low. It is likely that DFe depleted ACC waters from the Atlantic sector of the Southern Ocean, which were initially entrained in the east-flowing northern flank of the Weddell Gyre flow along the eastern flank of the Weddell Gyre (Figure 1a) southward toward Antarctica. While these low DFe waters become part of the west-flowing southeastern flank of the Weddell Gyre and the Antarctic Coastal Current, they hardly become enriched when flowing onto the narrow continental shelf of the southeastern Weddell Sea. *Klunder et al.* [2011] attributed low DFe observations close the Antarctic continent to the low carbon export flux to the sediment due to the presence of extended ice shelves in the region. The low organic carbon load to the sediment should result in a negligible benthic efflux of DFe into the bottom water. However, DFe could be low also due to scavenging from the upper water column by rising frazil ice during recent sea ice formation as evidenced by freezing temperatures (−1.86°C) in the upper 150 m [*Boyé et al.*, 2001] and a maximum in beam transmission as observed at ANT XVI/3 station 182 (data not shown). Recent seasonal sea ice formation is supported by the presence at the time of sampling at this station of grease ice, nilas and gray ice, which are young ice types [*Garrity*, 2000].

4. ANT X/6 stations 877, 879, 901, 903, 905, 907, 908, 947, 960, 964 and 972, located in the PFZ between the Polar Front (PF) and the Subantarctic Front (SAF) [*de Baar et al.*, 1995; *Löscher et al.*, 1997]. High DFe in these remote waters could be indicative of dust inputs from the Patagonian desert into the Subantarctic South Atlantic waters on the Falkland Plateau and could contribute as much as 0.05 to 0.2 μmol/m^2/d soluble Fe [*Gaiero et al.*, 2003]. Dust inputs of this magnitude are however sporadic and short-lived events [*Gassó and Stein*, 2007], but they could increase the DFe concentration in the upper 100 m by 0.05 to 0.2 nmol/L/d. This atmospheric signal could then be transported further east in the PF and the SAF, but it would only partly explain the higher observed DFe concentrations during the ANT X/6 cruise. As these fronts have been flowing across the North Scotia Ridge and over the extended continental shelf of the Falkland Plateau [*Orsi et al.*, 1995], these stations have likely received DFe from local sedimentary sources there and would belong to a different lateral diffusion/advection regime (e.g., higher flow rates in the Polar Front jet [*Hofmann*, 1985]) than that of the Peninsula area. The enhanced DFe observed in the northern part of the cruise tracks during the ANT X/6 cruise, would then have been further transported eastward along and across fronts [*de Baar et al.*, 1995] in mesoscale eddies, as proposed by *Kahru et al.* [2007]. Yet another intriguing explanation may be offered by the presence during ANT X/6 of

Table 2. Hydrographic Station Data by Cruise

Station	d Coastline[a] (km)	Bottom Depth (m)	UML Depth[b] (m)	Scale Length (km)	K_h [b] (m^2/s)	K_z [c] (cm^2/s)	Average [DFe] < 200 m (nmol/L)	[DFe] Base UML (nmol/L)	Average [DFe] in UML (nmol/L)	[DFe] at 300 m (nmol/L)
					ANT VII/3 EPOS					
153	240	3364	113	458	665	0.24	7.79	8.67	7.93	6.68
159	420	3899	53	802	1000	0.12	2.58	3.54	2.09	2.38
171	20	238	39	38	38	0.08	51.60	59.05	57.40	64.41
					ANT XXII/2 ISPOL					
011-3	72	4340	38	137	167	0.09	7.73	3.37	0.58	1.19
06-142	230	1412	33	439	633	0.18	0.75	0.91	3.37	12.06
					ANT X/6					
862	200	4872	69	382	539	0.12	0.65	0.57	0.89	0.77
865	640	4887	155	1222	1000	0.12	0.62	0.93	0.54	1.33
887	1250	3738	98	2386	1000	0.15	0.64	0.69	0.51	1.02
891	1330	3117	196	2539	1000	0.12	0.60	1.17	0.60	0.90
893	1350	2380	164	2577	1000	0.19	0.32	0.22	0.32	-
897	1450	2200	189	2768	1000	0.12	0.67	0.34	0.78	0.38
899	1500	2060	205	2863	1000	0.10	0.47	0.47	0.47	1.25
911	1250	4059	165	2386	1000	0.14	0.41	0.24	0.49	0.90
915	1220	2478	97	2329	1000	0.10	0.56	0.50	0.59	1.42
941	1220	3360	116	2329	1000	0.12	0.40	0.63	0.34	0.34
943	1250	3631	116	2386	1000	0.15	0.64	0.70	0.32	2.00
945	1330	3175	160	2539	1000	0.16	0.54	1.49	0.22	1.00
949	1400	2608	216	2672	1000	0.13	0.39	0.57	0.39	0.57
956	1570	2347	119	2997	1000	0.14	0.83	0.35	0.83	0.96
					ANT XIII/2					
5	2270	3800	121	4333	1000	0.18	0.31	0.27	0.28	0.40
8	1240	4863	50	2367	1000	0.14	0.43	0.42	0.32	0.67
9	1695	2753	149	3235	1000	0.13	0.32	0.33	0.32	0.51
10	2420	4350	218	4619	1000	0.16	0.30	0.17	0.26	0.28
13	2670	4178	36	5010	1000	0.11	0.15	0.16	0.20	0.21
15	2570	4102	34	4905	1000	0.13	0.15	0.22	0.23	0.19
16	2490	3992	60	4753	1000	0.14	0.10	0.09	0.10	0.19
18	2470	4279	63	4715	1000	0.12	0.17	0.18	0.18	0.22
19	2510	4014	63	4791	1000	0.10	0.14	0.15	0.18	0.16
20	2570	3560	54	4905	1000	0.10	0.13	0.09	0.18	0.19
21	2520	4063	58	4810	1000	0.13	0.08	0.08	0.09	0.18
25	2500	4243	54	4772	1000	0.14	0.14	0.21	0.17	0.18
29	2500	4041	65	4772	1000	0.16	0.18	0.15	0.20	0.28
32	2585	4173	78	5010	1000	0.14	0.13	0.13	0.14	0.21
					ANT XVI/3					
163	3220	4706	79	6146	1000	0.10	0.22	0.11	0.26	0.21
165	3195	4572	123	6098	1000	0.11	0.12	0.15	0.11	0.23
167	2920	4610	97	5573	1000	0.08	0.37	0.48	0.39	0.28
169	2470	4744	79	4715	1000	0.07	0.14	0.07	0.14	0.26
190	2855	3450	113	5449	1000	0.10	0.20	0.13	0.21	0.11
194	2850	4478	125	5440	1000	0.09	0.10	0.06	0.12	0.18
197	3020	3448	127	5764	1000	0.15	0.16	0.12	0.16	0.28
200	3220	4674	131	6146	1000	0.12	0.20	0.22	0.19	0.18
202	3250	4508	110	6203	1000	0.09	0.10	0.04	0.12	0.13
204	3270	4626	111	6241	1000	0.09	0.15	0.07	0.16	0.19
206	3370	5056	89	6432	1000	0.09	0.19	0.22	0.20	0.22
207	3520	4576	135	6719	1000	0.12	0.05	0.05	0.05	0.10

[a]Distance from the nearest Antarctic Peninsula, South Sandwich Islands, or western Weddell Sea shorelines. For stations in the ACC further away than 2000 km, the East Antarctic mainland (about 2000 km away) and South Africa (about 1800 km away) become closer than the West Antarctic continental shelves. However, in light of the general easterly circulation and limited cross-frontal exchange between the ACC and subtropical waters, we deem the distance to the West Antarctic continental shelves as the most relevant parameter.

[b]K_h was allowed to increase with scale length [*Okubo*, 1971] until a value of 1000 m^2/s [*Marshall et al.*, 2006] was reached.

[c]Derived from hydrographic data from *Strass* [2010], *Strass and Rohardt* [2010], *Absy et al.* [2008], *Smetacek et al.* [1997], and http://www.pangaea.de/search?q=@ref10037 (ANT VII/3).

exceptionally high numbers of icebergs in the ACC with higher DFe concentrations possibly due to increased melting in the warmer waters of the Polar Frontal Zone [*Smetacek et al.*, 2002]. The other ANT X/6 stations further to the south do fit the decreasing DFe trend: they are associated with waters between the PF and the Southern ACC Front (SACCF), which have had contact with the South Scotia Ridge, South Sandwich Arc and the island shelf of South Georgia.

5.2.2. Lateral DFe Input

[33] These observations suggest that the combination of extended shelves and rugged bottom topography in the

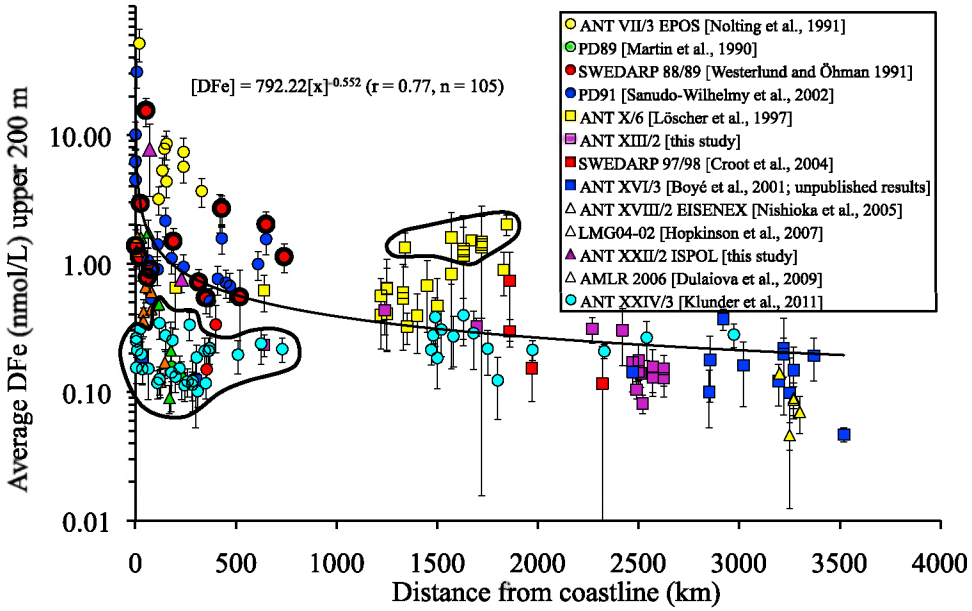

Figure 6. Exponential decrease of DFe (logarithmic scale) in the upper 200 m in the Atlantic sector of the Southern Ocean as a function of distance from the nearest Antarctic Peninsula, South Sandwich Islands, or western Weddell Sea shorelines (data in Table 2 and Table S1). The curve fit equation refers to x in meters. See section 5.2 for excluded data; excluded stations are encircled here as well as displayed within the rectangular boxes in Figure 1b. Error bars represent 1 x SD of the average DFe concentration in the upper 200 m and are deemed to reflect mostly natural variability and to a lesser extent analytical uncertainty.

Antarctic Peninsula and South Scotia Ridge area, with ACC and western Weddell Gyre in extensive contact with the shelves of the Antarctic Peninsula, and with the Weddell Gyre flowing out into the Scotia Sea, may cause large-scale DFe enrichment of pelagic waters downstream of the Antarctic Peninsula. The scatter seen at the shorter distances from shore (Figure 6) may be indicative of multiple sedimentary DFe sources with variable strengths at work. This variability may be due to the numerous islands offshore from the Antarctic Peninsula, the ruggedness of the coastline, as well as varying widths of the continental plateau [*Chase et al.*, 2005; *Bruland et al.*, 2001]. Also the load of organic matter to the sediment may vary from place to place, which will have repercussions on the local magnitude of the benthic flux of iron [*Elrod et al.*, 2004; *Schoemann et al.*, 1998]. It should be noted that biological uptake of DFe by phytoplankton followed by sedimentation below 200 m could also explain some of the variability.

[34] The offshore latitudinal horizontal transport of DFe in the Atlantic sector of the Southern Ocean can be estimated by applying the following one-dimensional advection/diffusion model [*Glover et al.*, 2011]:

$$\frac{\partial[DFe]}{\partial t} = -u\left(\frac{\partial[DFe]}{\partial x}\right) + K_h\left(\frac{\partial^2[DFe]}{\partial x^2}\right) + J_h \qquad (1)$$

which means that the rate of change of the DFe concentrations is equal to the sum of the horizontal advective flux divergence (left term), the horizontal eddy diffusive flux divergence (middle term) and a source/sink term (J_h). Under steady state conditions $\frac{\partial[DFe]}{\partial t} = 0$ and equation (1) can be rewritten as:

$$J_h = u\left(\frac{\partial[DFe]}{\partial x}\right) - K_h\left(\frac{\partial^2[DFe]}{\partial x^2}\right) \qquad (2)$$

The horizontal advective flux divergence (in μmol/m^3/s) is the product of the average zonal velocity u of the ACC (in m/s) and the slope of the DFe gradient (in μmol/m^4) with distance x from the source (in meters). The DFe gradient is best described according to the power function [DFe] = $792.22[x]^{-0.552}$ (r = 0.77, n = 105) (Figure 6). The term $\frac{\partial[DFe]}{\partial x}$ is found as the first derivative of this curve fit. The averaged zonal velocity u was obtained from *Best et al.* [1999] and was allowed to increase linearly across a continental shelf of 200 km wide [*Riffenburgh*, 2007] from 0.01 m/s [*Smith et al.*, 1999] to 0.06 m/s [*Best et al.*, 1999] in off-shelf waters and further away.

[35] The right term describes the horizontal eddy diffusive flux divergence [*Glover et al.*, 2011; *Sañudo-Wilhelmy et al.*, 2002; *Landing and Bruland*, 1987]. It is assumed that the apparent horizontal diffusion in latitudinal and meridional directions is equivalent. This latter assumption is ultimately flawed however, because of the predominantly easterly circulation in the ACC, but should serve as a first approximation due to a general lack of detailed long meridional transects. The apparent horizontal eddy diffusivity K_h depends on the scale length according to the empirical relationship $K_h = 0.103l^{1.15}$ (K_h in cm^2/s and scale length l in cm) [*Okubo*, 1971]. The scale length is defined as

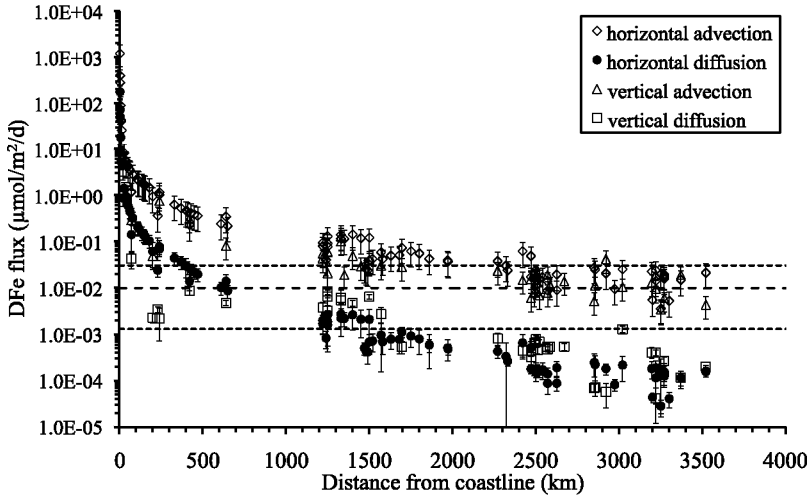

Figure 7. DFe fluxes of horizontal advection, horizontal diffusion, vertical advection, and vertical diffusion (in μmol/m^2/d) to the surface mixed layer in the Atlantic sector, Southern Ocean, as a function of distance from the nearest Antarctic Peninsula, South Sandwich Islands, or Weddell Sea shorelines. Note the logarithmic scale. Average atmospheric flux of 0.0099 μmol/m^2/d (see section 5.2) is indicated by a horizontal dashed line. Maximum and minimum atmospheric fluxes are indicated by dotted lines (see section 5.2).

the distance by which DFe decreases by 1/e of its initial concentration [*Johnson et al.*, 1997]. *Johnson et al.* [1997] obtained the scale length as the inverse slope of a linear relationship between ln(DFe) and distance from the Californian coast. In this study we found however a nonlinear function between ln(DFe) and distance from the Antarctic coast, given as y = 0.552ln[x] + 6.68, r = 0.77, n = 105. This function was used to calculate the scale length as the inverse slope of the tangent (first derivative) to this curve at every station and used this value to calculate K_h. The second derivative $\frac{\partial^2[DFe]}{\partial x^2}$ of the aforementioned power function between [DFe] and distance from the source will give the curvature of the horizontal DFe gradient [*Landing and Bruland*, 1987]. The product of K_h (m^2/s) and $\frac{\partial^2[DFe]}{\partial x^2}$ (in μmol/m^5) will yield the horizontal diffusion (in μmol/m^3/s).

[36] *Okubo*'s [1971] empirical relationship covers a range of scale lengths between 30 m and 100 km and a range of K_h between 0.05 and 220 m^2/s. *Marshall et al.* [2006] estimated the K_h distribution in the Southern Ocean from large-scale altimetry data and obtained values for the ACC of about 1000 m^2/s. This is similar to values reported for the North Atlantic Ocean [*Ledwell et al.*, 1998; *Sundermeyer and Price*, 1998] and indicates that *Okubo*'s [1971] empirical relationship could be extended beyond the given ranges and could still act at scales up to 1000 km (this is suggested in his Figure 4). Here, we let K_h increase with scale length according to *Okubo* [1971] until a value for K_h of 1000 m^2/s is reached (corresponding to a scale length of about 650 km), to remain constant at this value for larger scales.

[37] Multiplying the horizontal advection and diffusion fluxes with the upper mixed layer depth (UML) will give these fluxes into the mixed layer in μmol/m^2/d. For those stations with only a surface DFe value a constant UML depth of 100 m was assumed. For the stations where a vertical CTD profile was available, the UML depths were calculated by determining pycnocline depths. These were determined from analyses of the Brunt-Väisälä or buoyancy frequency N (in s^{-1}): $N^2 = \frac{g}{\rho}\frac{\partial \rho}{\partial z}$, where g is gravity (9.81 m/s^2), ρ is potential density and $\frac{\partial \rho}{\partial z}$ the density gradient [*Gargett*, 1984]. N^2 was calculated with 1 m resolution, while $\frac{\partial \rho}{\partial z}$ slopes were obtained over 5 m intervals. Only those values with r > 0.8 for $\frac{\partial \rho}{\partial z}$ over the 5 m intervals were taken. The pycnocline could then be identified as a peak of N^2 versus depth. The values for the stations distance to the coast, pycnocline depth, scale length and K_h are summarized in Table 2.

[38] Horizontal advection turns out to be more important than horizontal diffusion by a factor of about 10 at distances less than 100 km, increasing to a factor of 100 in the ACC. The modeled total horizontal flux (sum of advection and diffusion) varies from as high as 1375 μmol/m^2/d for the shortest distances from shore (within 5 km), to values of 5 μmol/m^2/d at 50 km, 2.5 μmol/m^2/d at 100 km and 1 μmol/m^2/d at 250 km (Figure 7). These values are in good agreement with a horizontal DFe flux of 1.8 μmol/m^2/d as determined by *Dulaiova et al.* [2009] for a 250 $\times$ 250 km area northeast of the tip of the Antarctic Peninsula. They used transects of short-lived radium isotopes and radium/iron ratios. These fluxes are higher than the horizontal fluxes of up to 0.39 μmol/m^2/d calculated for the island shelf system of the Crozet Islands, determined in a similar way with radium isotopes [*Charette et al.*, 2007; *Planquette et al.*, 2007]. This may be a consequence of the much less extensive shelf of the Crozet Islands, leading to less high DFe fluxes as compared with the Antarctic Peninsula region [*Chase et al.*, 2005].

[39] Open ocean horizontal flux decreases further with increasing distance from the continental shelf break to less than 0.02 μmol/m^2/d at the furthest positions eastward of the Antarctic Peninsula area (Figure 7).

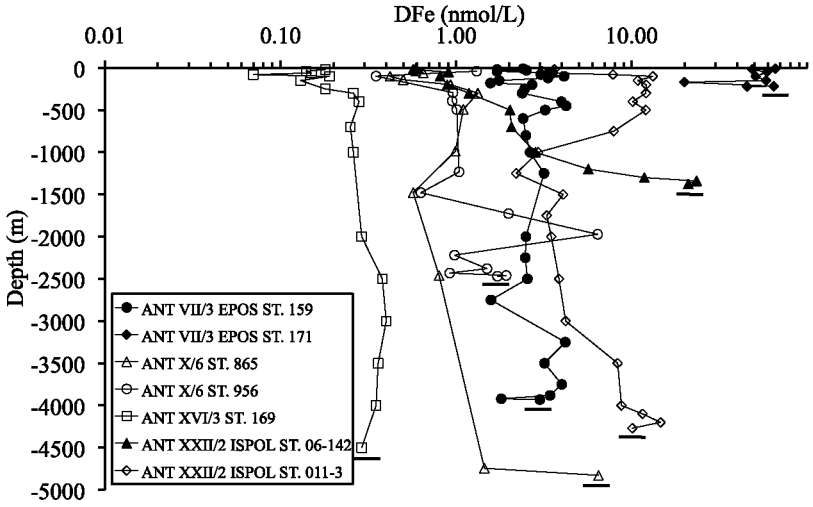

Figure 8. Compilation of surface-to-bottom vertical profiles of DFe in the Atlantic sector of the Southern Ocean illustrating the general decrease of DFe concentrations eastward of the Antarctic Peninsula. Data from ANT VII/3 [*Nolting et al.*, 1991], ANT X/6 [*Löscher et al.*, 1997], ANT XVI/3 [*Boyé et al.*, 2001], and ANT XXII/2 (this study). Note the logarithmic DFe scale. Black horizontal lines at the end of each profile indicate the seafloor at each station.

5.2.3. Benthic DFe Fluxes

[40] Fueling the calculated lateral DFe flux are most likely the sediments at the Antarctic continental shelves, therefore the benthic flux source term must be sufficiently high. There exists however a great lack of data on Southern Ocean sediment pore water DFe fluxes. There is also a paucity of complete water column profiles down to the seafloor, which could provide evidence of benthic DFe fluxes. Of the seven stations with DFe profiles down to the seafloor presented in Figure 8, four of them show indication of DFe enrichment on approaching the seafloor. We propose the use of the observed gradients of these near-bottom DFe profiles in combination with estimates of the abyssal vertical eddy diffusivity coefficient (K_z) to derive apparent DFe fluxes at the sediment-water interface. These four stations and their sediment derived DFe fluxes are displayed in Table 3. We used an abyssal K_z of 3.10^{-3} m^2/s [*Naveira Garabato et al.*, 2004; *Heywood et al.*, 2002]. The average sediment flux was found to be 9.2 ± 6.6 $\mu mol/m^2/d$, range 1.3–15.5 $\mu mol/m^2/d$ (Table 3). Similar sediment flux ranges were found on continental margins adjacent to ocean basins for the Pacific by *Elrod et al.* [2004] (range 1.3–10.8 $\mu mol/m^2/d$) and *Severmann et al.* [2010] (range 6–568 $\mu mol/m^2/d$), while *Blain et al.* [2008] reported a value for the subantarctic Kerguelen Island shelf of 136 $\mu mol/m^2/d$. Elsewhere, values for coastal marine sediments are not much different, e.g., *Pakhomova et al.* [2007] measured fluxes in the Gulf of Finland between 5 and 1000 $\mu mol/m^2/d$, while *Epping et al.* [1998] measured between 20 and 1440 $\mu mol/m^2/d$ in an intertidal area of the coastal North Sea. The formation of reduced soluble Fe in the sediment depends primarily on the load of organic matter and consequently the oxygen penetration depth [*Sachs et al.*, 2009, *Elrod et al.*, 2004, *Schoemann et al.*, 1998]. The diffusion of DFe across the sediment-water interface will depend on the oxygen concentration in the bottom water, bioirrigation, stabilizing of the Fe solubility by organic complexation, and sediment resuspension and redistribution [*Severmann et al.*, 2010; *Pakhomova et al.*, 2007; *Gerringa et al.*, 2008; *Elrod et al.*, 2004]. These factors determine if DFe will rapidly precipitate or adsorb to particles in the bottom waters, or will enter the ocean interior. Benthic DFe fluxes on continental margins or their slopes are likely responsible for fueling of the largest part if not all of the lateral DFe flux from the Antarctic Peninsula as estimated in this study.

5.2.4. Iron From Hydrothermal Sources and Volcanism

[41] Hydrothermal input has been proposed to be an important contributor to the DFe inventory of the Southern Ocean [*Tagliabue et al.*, 2010]. For instance, the possibility of hydrothermal venting near Bouvet Island in the Atlantic sector of the Southern Ocean had been discussed by *Croot et al.* [2004] and indeed evidence was found of inputs of DFe [*Klunder et al.*, 2011; *Löscher et al.*, 1997] and DMn [*Middag et al.*, 2011] in deep waters at the Bouvet Triple Junction Ridge. Hydrothermal sites have also been found in shallow waters of the Bransfield Strait area [*Klinkhammer et al.*, 2001]. High DFe of 31 nmol/L in the caldera of Deception Island of the South Shetland island group [*Sañudo-Wilhelmy et al.*, 2002] could be attributed to hydrothermal activity [*Rey et al.*, 1995]. *Yücel et al.* [2011] have highlighted the role of iron sulfide nanoparticles for the transport of iron away from hydrothermal vent sites, while *Sander and Koschinsky* [2011] showed that organic complexation could play a role in increasing hydrothermal DFe fluxes. Fluxes of hydrothermal DFe could locally attain

Table 3. Diffusive DFe Fluxes at the Sediment-Water Interface

Station	Diffusive Flux ($\mu mol/m^2/d$)
ISPOL 06-142	13.6
ISPOL 011-3	1.3
ANT X/6 865	15.5
ANT X/6 956	6.3

values up to 1 μmol/m^2/d [*Tagliabue et al.*, 2010] and could contribute in shallow waters to lateral DFe transport off the shelf, together with sediment sources of DFe. Finally, the South Sandwich Islands have been the scene of a major pumice eruption in the 1960s with the resulting pumice rafting its way around the Southern Ocean over the next few years [*Coombs and Landis*, 1966]. However, volcanic eruptions are sporadic, contrary to hydrothermal vents, which are relatively constant sources of DFe to the ocean interior on millennial timescales [*Tagliabue et al.*, 2010].

5.2.5. Iron From Below

[42] Vertical upward advective/diffusive flux estimates for the mixed layer can be calculated as by *Jickells* [1999]:

$$J_z = w[DFe]_{BML} + K_z\left(\frac{\partial[DFe]}{\partial z}\right) \quad (3)$$

Here, w is the upwelling velocity due to Ekman pumping, taken as 1.10^{-6} m/s (or 32 m/yr) from a modeling study of the Southern Ocean by *Ito et al.* [2005]. This is a reasonable value when compared with a natural radiotracer study by *Geibert et al.* [2002], who used ^{227}Ac to obtain an upwelling velocity in the eastern Weddell Sea of 55 $\pm$ 20 m/yr (or 1.7 10^{-6} m/s). $[DFe]_{BML}$ is the DFe concentration at the base of the mixed layer, K_z is the vertical eddy diffusivity (m^2/s) and $\frac{\partial[DFe]}{\partial z}$ the slope of DFe gradient versus depth (μmol/m^4). The buoyancy frequency N can here be used to parameterize vertical diffusivity with the empirical relation $K_z = a_0 N^{-q}$ with $q = 1$ and $a_0 = 10^{-7}$ m^2/s^2 [*Gargett*, 1984]. The results of the calculations are displayed in Table 4 and Figure 7. The values at each station for K_z and DFe concentration at the base of the upper mixed layer are summarized in Table 2. We found K_z in the pycnocline to vary between 1.10^{-5} and 2.10^{-5} m^2/s, which is in accordance with Southern Ocean canonical values from *Law et al.* [2003]. Our calculations indicate a more important role for vertical advection than for vertical diffusive flux. Vertical advection decreases from 5.1 μmol/m^2/d nearest to the Antarctic Peninsula to around 0.01 μmol/m^2/d in the open ocean, while the vertical diffusive flux decreases from 0.043 μmol/m^2/d to less than 0.001 μmol/m^2/d at the remotest stations.

5.2.6. The Role of Winter Convection

[43] Deep winter mixing could replenish DFe depleted surface waters with DFe enriched deeper water, and provide a new DFe inventory for the phytoplankton bloom of next spring. *Nishioka et al.* [2011] estimated winter mixing fluxes by comparing summer upper mixed layer DFe concentrations with winter DFe concentrations. As winter concentrations of DFe are not available yet for the Southern Ocean, due to the ocean's inaccessibility in winter, an alternative approach is to take a DFe concentration at a depth corresponding to the maximum winter mixing overturn. This DFe concentration at the assumed base of the winter mixed layer is presumably also the value that would be reached throughout the upper mixed layer at the end of the period of winter mixing. Winter mixing DFe flux was calculated for a period of 5 months (150 days) as follows [*Nishioka et al.*, 2011]:

$$J_{winter\ mixing} = (C_1 - C_2)z_{UML} \quad (4)$$

C_1 is the "winter concentration" at 300 m depth, C_2 is the average DFe concentration in the summer upper mixed layer and z_{UML} the summer upper mixed layer depth (see also Table 2). *Nishioka et al.* [2011] assumed that winter mixing replaces vertical advection and diffusion. We obtained a range of 0–1.9 μmol/m^2/d (disregarding some negative values). The results are summarized in Table 5 and are expressed as annual fluxes to estimate the percentage annual contribution. It appears that winter mixing contributes significantly to the upward flux of DFe to the upper mixed layer, but that judging from the negative values at some stations, downwelling of DFe could occur. Whether the latter is real or a serendipitous consequence of using summer data, remains unknown. In Table 5 these downwelling events are bracketed and for simplicity not taken into further consideration.

5.2.7. Iron From Above

[44] Atmospheric flux of DFe, J_{atm}, was estimated using the equation below and data from recent literature:

$$J_{atm} = S_{Fe}\frac{J_{dust}A_{Fe}}{M_{Fe}} \quad (5)$$

For the solubility of aerosol Fe, S_{Fe}, we chose a fixed value of 7 $\pm$ 3% averaging solubility data from *Baker et al.* [2006] for the southwestern South Atlantic. For the dust flux J_{dust} we averaged recent measurements by *Wagener et al.* [2008] (4 mg/m^2/yr for the Southeast Pacific and 14 mg/m^2/yr near the Kerguelen Archipelago in the Subantarctic Indian Ocean), *McConnell et al.* [2007] (27 mg/m^2/yr at James Ross Island, Antarctic Peninsula) and *Planquette et al.* [2007] (200 mg/m^2/yr at Crozet Islands, Subantarctic Indian Ocean). A_{Fe} is the crustal molar Fe abundance, 4.32% [*Wedepohl*, 1995], and M_{Fe} is the atomic weight of Fe. The mean soluble Fe input would amount to 0.0091 $\pm$ 0.0138 μmol/m^2/d to which an estimated 0.0008 $\pm$ 0.0004 μmol/m^2/d soluble Fe from extraterrestrial dust [*Johnson*, 2001] was added, totaling to 0.0099 $\pm$ 0.0138 μmol/m^2/d. Higher dust inputs can occur locally and sporadically, such as in the case of the Patagonian desert, which could contribute as much as 0.05 to 0.2 μmol/m^2/d soluble Fe to the South Atlantic waters on the Falkland Plateau [*Gaiero et al.*, 2003].

[45] Supporting generally low atmospheric inputs in Antarctica are values of 0.8 to 1.1 μmol/m^2/yr (0.002–0.003 μmol/m^2/d) of TD-Fe derived from ice cores at Law Dome, East Antarctica and marine and continental snow from around Antarctica [*Edwards et al.*, 2006; *Edwards and Sedwick*, 2001]. *Bowie et al.* [2009] estimated atmospheric DFe fluxes of 0.0024–0.0074 μmol/m^2/d for Southern Ocean waters near Tasmania. *Measures and Vink* [2000], who used seawater dissolved Al as a proxy of atmospheric dust, calculated a dust flux of 0.009 g/m^2/yr in the Ross Sea, which with 4.32% Fe abundance and 7% solubility would translate into a DFe flux of 0.001 μmol/m^2/d.

5.2.8. Uncertainty Budget

[46] We estimated combined uncertainties on the calculated fluxes by error propagation calculation. The results are summarized in Table 6. The uncertainties in the DFe supply by atmospheric deposition and by horizontal and vertical advection are the largest. To calculate vertical advection, we assumed a value for upwelling velocity, which is constant in space, time and direction. This is probably not the case in reality as there may be regional differences in upwelling

Table 4. Daily Horizontal and Vertical Fluxes of DFe in the Atlantic Sector of the Southern Ocean During Summer by Cruise

Station	d Coastline (km)	Horizontal Advection (SD) (μmol/m^2/d)	Vertical Advection (SD) (μmol/m^2/d)	Horizontal Diffusion (SD) (μmol/m^2/d)	Vertical Diffusion (SD) (μmol/m^2/d)	Total Flux[a] (SD) (μmol/m^2/d)	Potential New PP (SD) (g C/m^2/d)	Literature PP (g C/m^2/d)
				ANT VII/3 EPOS				
153	240	1.15 (0.63)	0.75 (0.38)	0.078 (0.026)	0.0022 (0.0015)	1.99 (0.73)	0.60 (0.37)	0.1–1.8[b]
159	420	0.23 (0.12)	0.31 (0.15)	0.014 (0.005)	0.0087 (0.0017)	0.56 (0.20)	0.17 (0.10)	0.3–1[c]
171	20	4.7 (2.6)	5.1 (2.6)	0.87 (0.30)	-	10.7 (3.7)	3.2 (1.9)	
				ANT XXII/2 ISPOL				
011-3	72	1.17 (0.64)	0.29 (0.13)	0.14 (0.08)	0.043 (0.018)	1.65 (0.67)	0.50 (0.32)	
06-142	230	0.36 (0.20)	0.078 (0.039)	0.024 (0.007)	0.0034 (0.0005)	0.47 (0.20)	0.14 (0.09)	
				ANT X/6				
862	200	0.93 (0.51)	0.049 (0.025)	0.061 (0.034)	0.0023 (0.0005)	1.05 (0.51)	0.32 (0.22)	0.3–3[d]
865	640	0.34 (0.19)	0.080 (0.022)	0.014 (0.005)	0.0048 (0.0006)	0.45 (0.19)	0.14 (0.09)	
887	1250	0.077 (0.042)	0.060 (0.030)	0.0016 (0.0008)	0.0066 (0.0025)	0.15 (0.05)	0.19 (0.11)	
891	1330	0.14 (0.08)	0.10 (0.05)	0.0027 (0.0018)	0.0054 (0.0040)	0.26 (0.09)	0.31 (0.19)	
893	1350	0.11 (0.06)	0.019 (0.010)	0.0022 (0.0007)	-	0.15 (0.06)	0.17 (0.12)	
897	1450	0.12 (0.06)	0.029 (0.015)	0.0021 (0.0013)	-	0.16 (0.07)	0.19 (0.13)	
899	1500	0.12 (0.07)	0.041 (0.020)	0.0021 (0.0014)	0.0064 (0.0007)	0.18 (0.07)	0.22 (0.14)	
911	1250	0.13 (0.07)	0.021 (0.010)	0.0027 (0.0014)	0.0032 (0.0028)	0.17 (0.07)	0.20 (0.13)	
915	1220	0.079 (0.043)	0.043 (0.022)	0.0017 (0.0007)	0.0038 (0.0011)	0.14 (0.05)	0.17 (0.10)	
941	1220	0.095 (0.052)	0.054 (0.010)	0.0020 (0.0010)	-	0.16 (0.06)	0.19 (0.12)	
943	1250	0.091 (0.050)	0.060 (0.030)	0.0019 (0.0013)	0.0083 (0.0012)	0.17 (0.06)	0.21 (0.13)	
945	1330	0.11 (0.06)	0.13 (0.07)	0.0022 (0.0027)	0.0062 (0.0027)	0.26 (0.09)	0.31 (0.19)	
949	1400	0.14 (0.08)	0.049 (0.025)	0.0026 (0.0014)	0.0047 (0.0007)	0.21 08)	0.25 (0.16)	
956	1570	0.058 (0.032)	0.030 (0.015)	0.00096 (0.00081)	0.0027 (0.0010)	0.10 (0.04)	0.12 (0.08)	
				ANT XIII/2				
5	2270	0.038 (0.021)	0.023 (0.012)	0.00043 (0.00013)	0.0008 (0.0002)	0.072 (0.027)	0.086 (0.054)	0.2–0.9[e]
8	1240	0.040 (0.022)	0.036 (0.018)	0.00083 (0.00034)	0.0023 (0.0006)	0.089 (0.032)	0.11 (0.07)	
9	1695	0.073 (0.040)	0.029 (0.014)	0.00111 (0.00027)	0.0005 (0.0002)	0.11 (0.04)	0.14 (0.09)	
10	2420	0.061 (0.034)	0.015 (0.007)	0.00066 (0.00033)	0.0004 (0.0001)	0.087 (0.037)	0.10 (0.07)	
13	2670	0.009 (0.005)	0.014 (0.007)	0.00009 (0.00003)	0.0005 (0.0001)	0.033 (0.016)	0.040 (0.028)	
15	2570	0.009 (0.005)	0.019 (0.010)	0.00009 (0.00004)	0.0005 (0.0001)	0.038 (0.017)	0.046 (0.031)	
16	2490	0.016 (0.009)	0.008 (0.004)	0.00017 (0.00004)	0.0006 (0.0001)	0.035 (0.017)	0.042 (0.029)	
18	2470	0.017 (0.009)	0.016 (0.008)	0.00018 (0.00004)	0.0004 (0.0001)	0.043 (0.018)	0.052 (0.034)	
19	2510	0.017 (0.009)	0.013 (0.007)	0.00017 (0.00005)	0.0005 (0.0001)	0.040 (0.018)	0.048 (0.032)	
20	2570	0.014 (0.008)	0.008 (0.004)	0.00014 (0.00005)	0.0005 (0.0001)	0.032 (0.016)	0.039 (0.027)	
21	2520	0.015 (0.008)	0.007 (0.003)	0.00016 (0.00004)	0.0007 (0.0001)	0.033 (0.017)	0.040 (0.028)	
25	2500	0.014 (0.008)	0.018 (0.009)	0.00015 (0.00005)	0.0007 (0.0001)	0.043 (0.018)	0.052 (0.034)	
29	2500	0.017 (0.010)	0.013 (0.007)	0.00018 (0.00006)	0.0008 (0.0002)	0.041 (0.018)	0.049 (0.033)	
32	2585	0.019 (0.011)	0.011 (0.006)	0.00019 (0.00007)	0.0005 (0.0001)	0.041 (0.018)	0.049 (0.033)	
				ANT XVI/3				
163	3220	0.014 (0.008)	0.010 (0.005)	0.00011 (0.00008)	0.0004 (0.0001)	0.034 (0.017)	0.041 (0.029)	
165	3195	0.022 (0.012)	0.013 (0.007)	0.00018 (0.00007)	0.0004 (0.0001)	0.046 (0.020)	0.055 (0.036)	
167	2920	0.020 (0.011)	0.041 (0.021)	0.00018 (0.00005)	0.00006 (0.00003)	0.072 (0.027)	0.086 (0.054)	
169	2470	0.049 (0.027)	0.006 (0.003)	0.00051 (0.00018)	0.0003 (0.0001)	0.066 (0.030)	0.079 (0.054)	
190	2855	0.025 (0.014)	0.011 (0.005)	0.00022 (0.00013)	0.00007 (0.00003)	0.046 (0.020)	0.055 (0.037)	
194	2850	0.027 (0.015)	0.005 (0.003)	0.00025 (0.00013)	0.00007 (0.00001)	0.043 (0.021)	0.051 (0.036)	
197	3020	0.025 (0.014)	0.010 (0.005)	0.00022 (0.00012)	0.0013 (0.0002)	0.047 (0.020)	0.057 (0.037)	
200	3220	0.024 (0.013)	0.019 (0.010)	0.00019 (0.00007)	0.00004 (0.00003)	0.053 (0.021)	0.063 (0.041)	

Table 4. (continued)

Station	d Coastline (km)	Horizontal Advection (SD) (μmol/m^2/d)	Vertical Advection (SD) (μmol/m^2/d)	Horizontal Diffusion (SD) (μmol/m^2/d)	Vertical Diffusion (SD) (μmol/m^2/d)	Total Flux[a] (SD) (μmol/m^2/d)	Potential New PP (SD) (g C/m^2/d)	Literature PP (g C/m^2/d)
202	3250	0.020 (0.011)	0.003 (0.002)	0.00016 (0.00014)	0.00017 (0.00002)	0.033 (0.018)	0.040 (0.029)	
204	3270	0.020 (0.011)	0.006 (0.003)	0.00015 (0.00008)	0.0003 (0.0001)	0.036 (0.018)	0.043 (0.030)	
206	3370	0.015 (0.008)	0.019 (0.010)	0.00012 (0.00005)	0.00012 (0.00004)	0.044 (0.019)	0.053 (0.035)	
207	3520	0.021 (0.012)	0.004 (0.002)	0.00016 (0.00003)	0.00020 (0.00001)	0.036 (0.018)	0.043 (0.031)	
Average contribution		54% (15%)	29% (13%)	1% (2%)	1% (1%)			
Atmospheric contribution		15% (10%)						

[a]Total DFe flux includes 0.0099 ± 0.0138 μmol/m^2/d atmospheric DFe flux.
[b]*Mathot et al.* [1992].
[c]*Korb et al.* [2005].
[d]*Jochem et al.* [1995].
[e]*Bracher et al.* [1999].

rates [*Ito et al.*, 2005]. Also the chosen average zonal velocity of the ACC to obtain the horizontal advection will have in reality a considerable variation in time and space. In this respect we point at the frontal jets in the oceanographic fronts, which can attain speeds of for instance up to 0.4 m/s in the Polar Front [*Hofmann*, 1985]. In between fronts, flow velocities are much lower. Regarding atmospheric input, we assumed for lack of observations an average atmospheric input everywhere, which in reality will be highly heterogeneous in magnitude, duration and area.

5.3. Additional DFe Sources

5.3.1. Iceberg Melting

[47] Icebergs are known to exert an influence on phytoplankton growth along the paths of drifting icebergs, which is thought to be due to the release of dissolved and particulate Fe by ice melt [*Schwarz and Schodlok*, 2009]. It has been argued that melting of calved icebergs could provide bioavailabe Fe by desorption of Fe oxyhydroxide nanoparticles associated with sediment and atmospheric dust entrained into the glacial ice [*Raiswell et al.*, 2008]. *Raiswell et al.* [2008] estimated that dissolution of nanoparticulate amorphous Fe oxyhydroxides associated with ice-trapped sediment in melting icebergs might add as much as 1.6 Gmol/yr potentially bioavailable Fe or 0.13 μmol/m^2/d for the whole Southern Ocean (surface area 34 million km^2 [*Arrigo et al.*, 2008]). This estimate hinges on an ascorbate extraction of these sedimentary nanoparticles, of which it is assumed that 5%–10% would be potentially bioavailable through dissociation of the nanoparticles from the sediment upon entering into contact with seawater or after biological processing by zooplankton grazing. This seems to be supportive to the observations by *Smith et al.* [2007] of higher productivity in the immediate vicinity of icebergs in neritic Antarctic Peninsula waters. A recent model study suggested that in areas where icebergs are present, 25% of Chl *a* could be attributed to DFe released by iceberg melting [*Lancelot et al.*, 2009]. Waters sampled around an iceberg in the Polar Front well away from continental Fe sources exhibited a heterogeneous TD-Fe distribution of 1–9 nmol/L [*Löscher et al.*, 1997], indeed suggesting a potential Fe input from icebergs. Moreover, recent results from the 2007 SIMBA cruise (RV *Nathaniel B. Palmer*) in the remote Bellingshausen Sea (J. de Jong, manuscript in preparation, 2012) showed enhancement by 0.3 nmol/L DFe and 0.5 nmol/L TD-Fe above subnanomolar background levels in the wake of an iceberg sampled at close vicinity, notably at the depths were the keel of the iceberg was suspected (250 m). Given the hydrographic situation in this latter case, with the keel of the iceberg in the warm core (+2°C) of the CDW, melting would indeed be greatest at this depth. However, the melting took place below the euphotic zone and would therefore have been of little benefit to primary producers unless these Fe enriched waters would be advected to the surface mixed layer further away. *Lin et al.* [2011] measured DFe in the waters surrounding several icebergs near the Antarctic Peninsula and observed that the highest DFe surface concentrations were associated with lower salinities, regardless of distance from the icebergs. This might indeed indicate that meltwater from iceberg could reach the surface by vertical mixing. It thus appears that icebergs could be a source of dissolved and particulate Fe, but issues like the magnitude of this Fe flux,

Table 5. Annual Horizontal and Vertical Fluxes of DFe (Including Winter Mixing) in the Atlantic Sector of the Southern Ocean by Cruise

Station	d Coastline (km)	Horizontal Advection (SD) (μmol/m^2/yr)	Vertical Advection 215 d (SD) (μmol/m^2/yr)	Horizontal Diffusion (SD) (μmol/m^2/yr)	Vertical Diffusion 215 d (SD) (μmol/m^2/yr)	Winter Mixing 150 d (SD) (μmol/m^2/yr)	Total Flux[a] (SD) (μmol/m^2/yr)
				ANT VII/3 EPOS			
153	240	419 (230)	161 (81)	28 (10)	0.5 (0.3)	(−141) (43)	612 (248)
159	420	82 (45)	66 (33)	5.1 (1.9)	1.9 (0.4)	16 (3)	174 (57)
171	20	1708 (942)	1097 (551)	318 (110)	-	273 (62)	3400 (1099)
				ANT XXII/2 ISPOL			
011-3	72	426 (235)	58 (29)	51 (31)	9.3 (3.8)	23 (2)	576 (239)
06-142	230	131 (72)	17 (8)	8.8 (2.6)	0.7 (0.1)	287 (39)	448 (83)
				ANT X/6			
862	200	339 (187)	11 (5)	22 (12)	0.5 (0.1)	(−8) (5)	376 (187)
865	640	125 (69)	9 (5)	5.1 (1.9)	1.0 (0.1)	122 (24)	275 (74)
887	1250	28 (15)	13 (6)	0.58 (0.29)	1.4 (0.5)	50 (16)	97 (24)
891	1330	51 (28)	22 (11)	0.99 (0.67)	1.2 (0.9)	60 (39)	138 (49)
893	1350	42 (23)	4 (2)	0.80 (0.27)	-	(−53) (15)	50 (28)
897	1450	43 (24)	6 (3)	0.77 (0.46)	-	(−76) (37)	54 (45)
899	1500	44 (24)	9 (4)	0.76 (0.50)	1.4 (0.2)	160 (102)	219 (105)
911	1250	47 (26)	4 (2)	0.98 (0.50)	0.7 (0.6)	68 (26)	125 (37)
915	1220	29 (16)	9 (5)	0.61 (0.25)	0.8 (0.2)	81 (39)	124 (43)
941	1220	34 (19)	4 (2)	0.73 (0.36	-	0 (-)	51 (20)
943	1250	33 (18)	13 (7)	0.69 (0.48)	1.8 (0.2)	195 (70)	247 (72)
945	1330	42 (23)	28 (14)	0.81 (1.00)	1.3 (0.6)	25 (101)	200 (105)
949	1400	52 (28)	11 (5)	0.96 (0.50)	1.0 (0.2)	38 (19)	106 (35)
956	1570	21 (12)	6.5 (3.3)	0.35 (0.29)	0.6 (0.2)	15 (13)	48 (18)
				ANT XIII/2			
5	2270	14 (8)	5.0 (2.5)	0.16 (0.05)	0.17 (0.05)	15 (2)	37 (10)
8	1240	14 (8)	7.8 (3.9)	0.30 (0.12)	0.5 (0.1)	18 (8)	44 (13)
9	1695	27 (15)	6.1 (3.1)	0.41 (0.10)	0.12 (0.03)	28 (5)	65 (17)
10	2420	22 (12)	3.2 (1.6)	0.24 (0.12)	0.09 (0.03)	4 (1)	33 (13)
13	2670	3.3 (1.8)	3.0 (1.5)	0.03 (0.01)	0.12 (0.02)	1 (0.1)	11 (6)
15	2570	3.2 (1.8)	4.1 (2.1)	0.03 (0.01)	0.12 (0.02)	(−1.4) (0.1)	11 (6)
16	2490	5.9 (3.2)	1.7 (0.8)	0.06 (0.01)	0.14 (0.03)	5 (0.7)	17 (6)
18	2470	6.3 (3.4)	3.3 (1.7)	0.07 (0.01)	0.09 (0.01)	3 (0.2)	16 (6)
19	2510	6.1 (3.4)	2.8 (1.4)	0.06 (0.02)	0.10 (0.02)	(−0.9) (0.1)	13 (6)
20	2570	5.1 (2.8)	1.7 (0.8)	0.05 (0.02)	0.10 (0.01)	1 (0.0)	11 (6)
21	2520	5.6 (3.1)	1.5 (0.7)	0.06 (0.01)	0.15 (0.01)	5 (0.7)	16 (6)
25	2500	5.3 (2.9)	3.9 (2.0)	0.05 (0.02)	0.14 (0.02)	1 (0.1)	14 (6)
29	2500	6.3 (3.5)	2.8 (1.4)	0.07 (0.02)	0.17 (0.03)	5 (1)	18 (6)
32	2585	7.1 (3.9)	2.4 (1.2)	0.07 (0.02)	0.11 (0.03)	6 (2)	19 (7)
				ANT XVI/3			
163	3220	5.2 (2.9)	2.0 (1.0)	0.04 (0.03)	0.09 (0.01)	(−4) (2)	11 (6)
165	3195	8.2 (4.5)	2.8 (1.4)	0.07 (0.03)	0.09 (0.02)	14 (6)	29 (9)
167	2920	7.4 (4.1)	8.9 (4.5)	0.07 (0.02)	0.01 (0.01)	(−10) (2)	20 (8)
169	2470	18 (10)	1.3 (0.7)	0.19 (0.07)	0.07 (0.02)	10 (3)	33 (12)
190	2855	9.0 (4.9)	2.0 (1.0)	0.08 (0.05)	0.02 (0.01)	(−11) (5)	15 (9)
194	2850	10 (5.5)	1.1 (0.6)	0.09 (0.05)	0.015 (0.003)	8 (4)	23 (8)
197	3020	9.3 (5.1)	2.2 (1.1)	0.08 (0.04)	0.28 (0.04)	15 (9)	31 (12)
200	3220	8.6 (4.7)	4.1 (2.1)	0.07 (0.03)	0.01 (0.01)	(−1.3) (0.6)	16 (7)
202	3250	7.2 (3.9)	0.7 (0.4)	0.06 (0.05)	0.04 (0.01)	1 (0.9)	13 (6)
204	3270	7.1 (3.9)	1.3 (0.7)	0.06 (0.03)	0.06 (0.01)	4 (2)	16 (7)
206	3370	5.5 (3.0)	4.1 (2.1)	0.04 (0.02)	0.03 (0.01)	2 (0.8)	15 (6)
207	3520	7.8 (4.3)	0.9 (0.5)	0.06 (0.01)	0.043 (0.002)	7 (1)	20 (7)
Average contribution		44% (17%)	15% (10%)	1% (2%)	0.6% (0.4%)	34% (21%)	
Atmospheric contribution		13% (11%)					

[a]Total DFe flux includes 3.6 ± 5.0 μmol/m^2/yr atmospheric flux.

whether this Fe is (bio)available, to which extent it will be scavenged and lost through sedimentation, and how large an area of the Southern Ocean could be fertilized, are all still to be dealt with.

5.3.2. Basal Ice Melting

[48] Draining of bedrock by Antarctic ice sheet meltwater, could provide 0.054 Gmol/yr DFe to Antarctic coastal waters [*Statham et al.*, 2008], or a horizontal flux of 78 μmol/m^2/d DFe if this mass passes through a surface determined by the circumference of the Antarctic coastline (roughly 19000 km) and a water depth of 100 m. This represents a contribution of ~6% to the lateral flux directly at the coast derived from terrestrial sources. It is probably not relevant at greater distances from the coast, where this signal is diluted further

Table 6. Estimated Uncertainties in the DFe Fluxes

Parameter	Unit	Median Coefficient of Variance (%)	Range Coefficient of Variance (%)
Upper mixed layer	m	2	1–10
Distance coastline	m	1	
Width continental shelf	m	25	
Average [DFe] < 200 m	nmol/L	25	11–129
[DFe] at base upper mixed layer	nmol/L	5	
Average [DFe] in upper mixed layer	nmol/L	35	3–84
[DFe] at 300 m	nmol/L	5	
Scale length	m	8	
K_h	m^2/s	8	
K_z	m^2/s	9	3–30
Zonal velocity ACC	m/s	53	
Upwelling velocity	m/s	50	
Slope [DFe] versus depth	$\mu mol/m^4$	19	1–86
Slope [DFe] versus distance source	$\mu mol/m^4$	15	
Curvature [DFe] versus distance source	$\mu mol/m^5$	17	
Fe/C ratios	μmol Fe/mol C	50	
Derived parameters			
Horizontal diffusion	$\mu mol/m^2/d$	32	22–130
Horizontal advection	$\mu mol/m^2/d$	55	55–56
Vertical diffusion	$\mu mol/m^2/d$	21	4–87
Vertical advection	$\mu mol/m^2/d$	50	
Winter convection	$\mu mol/m^2/yr$	36	7–85
Atmospheric dust	$\mu mol/m^2/d$	152	
Interplanetary dust	$\mu mol/m^2/d$	50	
Total flux	$\mu mol/m^2/d$	43	34–53
New primary productivity	g $C/m^2/d$	66	61–73

away from its source, while over the outer shelf the sediment is present as the dominating DFe source.

5.3.3. Sea Ice Melting

[49] Antarctic and Arctic sea ice have been shown to exhibit dissolved and particulate Fe concentrations one to two orders of magnitude higher than underlying seawater [*van der Merwe et al.*, 2011; *Lannuzel et al.*, 2010, 2008, 2007; *Tovar-Sánchez et al.*, 2010; *Aguilar-Islas et al.*, 2008]. By budget estimate it was concluded that most of the Fe accumulated in Antarctic seasonal sea ice must have come from an upwelling supply of Fe from deeper waters [*Lannuzel et al.*, 2010, 2008, 2007]. This implies a hitherto not fully understood scavenging mechanism to build up Fe into the sea ice during the autumn season of formation of new sea ice [*Lannuzel et al.*, 2010]. With its high Fe concentrations, sea ice can be regarded as a potential source of Fe during ice melt. It was demonstrated for the Weddell Sea by *Lannuzel et al.* [2008] that during sea ice melting, DFe became depleted in the ice within 1 month at a rate of 0.38 $\mu mol/m^2/d$. Estimated sea ice inputs by *Lannuzel et al.* [2007] for East Antarctica of 0.30 $\mu mol/m^2/d$, and by *Croot et al.* [2004], 0.03–1.5 $\mu mol/m^2/d$, were of a similar order, assuming a melt period of 1 month. The DFe thus released into the surface ocean is also likely to be bioavailable due to the high concentrations of saccharides in sea ice [*Dumont et al.*, 2009], which render DFe more bioavailable than other naturally occurring organic ligands [*Hassler et al.*, 2011; *Hassler and Schoemann*, 2009]. This DFe would be supplied to the surface of the open ocean in spring and in combination with the improving light conditions and water column stability, could be instrumental in triggering widespread phytoplankton blooms along the retreating sea ice edge and in polynyas (Figure 1a).

5.4. Relative Importance of DFe Fluxes

[50] The relative contribution of each DFe flux to the total DFe input in summer indicates that horizontal advection is dominating throughout at 54 ± 15% (Table 4), followed by vertical advection at 29 ± 13%. Horizontal and vertical diffusion contribute at 1 ± 2% and 1 ± 1%, respectively. Atmospheric flux increases in importance from negligible close to the Antarctic continent to third most important DFe supplier in the remote open ocean at 15 ± 10%. This pattern changes somewhat on an annual timescale when we consider deep winter mixing, which replaces vertical advection and vertical diffusion during the winter months, leading to annual contributions to the upper mixed layer DFe inventory (Table 5) of horizontal advection of 44 ± 17%, winter convection (150 days) of 34 ± 21%, vertical advection (215 days) of 15 ± 10%, horizontal diffusion of 1 ± 2%, vertical diffusion (215 days) of 0.6 ± 0.4%, and atmospheric flux of 13 ± 11%. Winter mixing increases the overall DFe flux into the upper mixed layer and could be an important source for DFe scavenging into sea ice during its formation [*Lannuzel et al.*, 2010].

[51] A conceptual diagram is given in Figure 9 summarizing DFe inputs, fluxes and delivery mechanisms.

5.5. Primary Productivity in the Atlantic sector of the Southern Ocean and Fe Fixation

[52] The observed primary productivity in the ocean areas investigated here ranges from low 0.1–0.3 g $C/m^2/d$ in the ACC until 1–3 g $C/m^2/d$ in frontal systems or in coastal waters [*Mathot et al.*, 1992; *Jochem et al.*, 1995; *Bracher et al.*, 1999; *Froneman et al.*, 2004; *Korb et al.*, 2005]. In order to transfer our DFe flux estimates into a Fe sustained

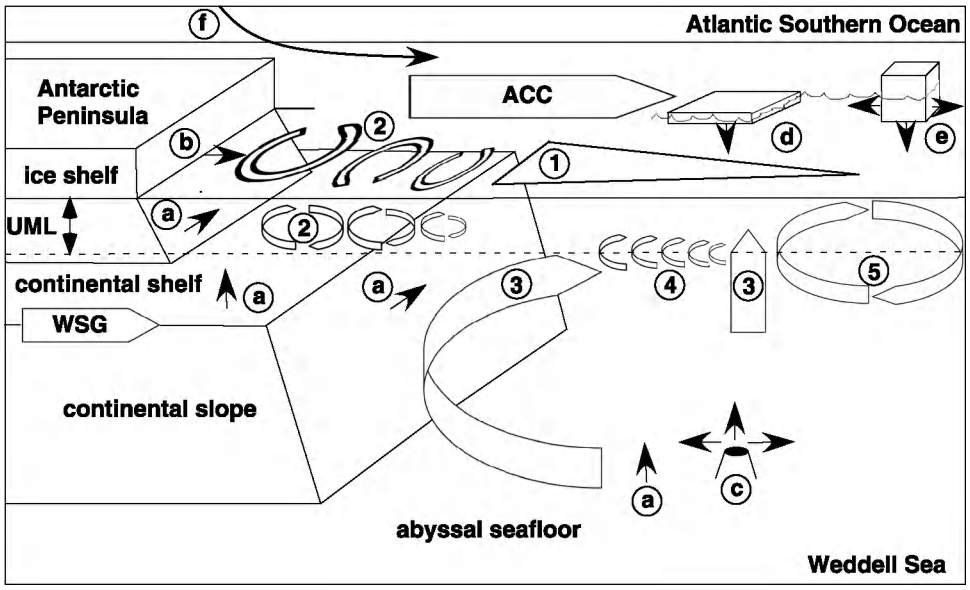

Figure 9. Simplified conceptual diagram summarizing DFe inputs, fluxes, and delivery pathways to the upper mixed layer. West is left. ACC, Antarctic Circumpolar Current; UML, upper mixed layer; WSG, Weddell Sea Gyre. The following DFe inputs can be discerned: a, benthic flux by sediment resuspension and diffusion (1.3–15.5 μmol/m^2/d, values as high as 1440 μmol/m^2/d have been reported elsewhere, see section 5.2); b, basal ice melting (78 μmol/m^2/d); c, hydrothermal activity (1 μmol/m^2/d); d, iceberg melting (0.13 μmol/m^2/d); e, sea ice melting (0.3–1.5 μmol/m^2/d); f, atmospheric input (0.01 μmol/m^2/d). Delivery pathways are as follows: 1, horizontal advection (0.02–1200 μmol/m^2/d); 2, horizontal diffusion (0.0002–177 μmol/m^2/d) through mesoscale eddies and turbulence in the upper mixed layer; 3, vertical advection of DFe enriched deep water (0.01–5.1 μmol/m^2/d); 4, vertical diffusion (0.001–0.04 μmol/m^2/d); 5, deep winter mixing (0–1.9 μmol/m^2/d).

new primary productivity we first have to assume Fe requirements for primary producers. We chose values for Fe/C of 40 μmol Fe: mol C for Fe replete conditions and 10 μmol Fe: mol C for Fe depleted ocean regions following estimations in the work of *Hassler and Schoemann* [2009], *de Baar et al.* [2008], *Sarthou et al.* [2005] and *Twining et al.* [2004]. We allowed for an uncertainty on the Fe/C ratios of 50% to respect the reported range of values in aforementioned references. Together with the uncertainty of the total DFe flux this results in a combined uncertainty of 66% (Tables 4 and 6).

[53] The primary productivity that could potentially be sustained by new DFe delivered to the Southern Ocean as calculated here for distances within 750 km offshore (mean 0.72 g C/m^2/d, range 0.14–3.2 g C/m^2/d), coincides with published values for the continental shelf and near margin stations in the Scotia Sea, but falls short of field measurements in the abyssal open Atlantic sector of the Southern Ocean (mean 0.11 g C/m^2/d, range 0.04–0.31 g C/m^2/d) (Table 4). Although we cannot exclude the possibility that this discrepancy is due to the inherent uncertainties of our estimations, it seems to imply that regenerated DFe may be an important source of DFe for sustaining primary productivity [*Boyd and Ellwood*, 2010]. This can be further corroborated by calculating the Fe fixation of primary producers as a function of their mean daily primary production, which is in shelf waters of the Weddell Sea sector 338 mg C/m^2/d, and in the pelagic waters 183 mg C/m^2/d [*Arrigo et al.*, 2008]. This productivity can be translated into Fe fixation on the continental shelf and the abyssal ocean using the Fe/C ratios from above. In this way it can be estimated that on the shelf 1.13 μmol/m^2/d Fe and in the pelagic waters 0.15 μmol/m^2/d Fe is fixed by primary producers. If we compare these Fe fixation rates with the actual average new DFe supply to the upper mixed layer within 750 km offshore of 2.4 μmol/m^2/d, then the supply is in excess of fixation with a factor of 2. This incomplete utilization of DFe could be caused by light limitation due to ice cover or algal self-shading in the Marginal Ice Zone (MIZ), or could be due to not all the DFe being bioavailable. Beyond 750 km offshore the average new DFe flux is 0.09 μmol/m^2/d, which means that fixation is a factor of 1.7 larger than the supply. The latter means that about 40% of the Fe fixation needs to be balanced by way of regenerative cycling flux [*Strzepek et al.*, 2005], which translates in a "*fe*" ratio of 0.59 ("*fe*" = uptake of new iron/uptake of new + regenerated iron) [*Boyd et al.*, 2005]. However, if we take into account maximum primary production rates of 1200 mg C/m^2/d in shelf waters, and 400 mg C/m^2/d in the open Southern Ocean [*Arrigo et al.*, 2008], then Fe fixation is higher at 4.0 and 0.33 μmol/m^2/d Fe, respectively. The new DFe supply on the shelf could become insufficient to sustain primary productivity at its maximum, expressed as a "*fe*" of 0.60, while in open ocean waters "*fe*" decreases to 0.27. Thus also in nearshore waters recycling could play a role of importance.

[54] Our "*fe*" values are higher than values of 0.17 in waters off New Zealand [*Boyd et al.*, 2005], 0.09–0.27 (mean 0.18) in the Southern Ocean south of Australia [*Bowie et al.*, 2001], 0.06–0.16 (mean 0.10) in the Southern Ocean near Tasmania [*Bowie et al.*, 2009], and 0.07–0.66 (mean 0.15) in the Northeast Atlantic [*de Jong et al.*, 2007]. It is closer to values of 0.39–0.58 (mean 0.49) above the Kerguelen plateau [*Sarthou et al.*, 2008]. These higher "*fe*" ratios are indicative of the presence of sources of new DFe [*Sarthou et al.*, 2008]. In any case, Fe recycling in the surface mixed layer is a key pathway by which Fe shortage could be replenished. The most likely route is via zooplankton grazing and there are a number of recent key laboratory [*Barbeau et al.*, 1996] and field studies [*Sarthou et al.*, 2008; *Tovar-Sánchez et al.*, 2007] pointing at this. For instance, *Barbeau et al.* [1996] reported digestion of colloidal iron in the acidic food vacuoles of protozoan grazers as a mechanism for the generation of "bioavailable" iron from refractory iron phases. *Sarthou et al.* [2008] showed that on the Kerguelen plateau copepod grazing had a strong impact on Fe regeneration, which accounted for half of the Fe demand. *Tovar-Sánchez et al.* [2007] proposed krill as a "major node" in Fe recycling, due to its high excretion rates of DFe. Interestingly, krill has even been proposed as a vector of new DFe to the upper mixed layer [*Schmidt et al.*, 2011], due to their seabed migration and foraging behavior in waters of 200–2000 m deep, where they ingest lithogenic particles. *Schmidt et al.* [2011] estimate that 0.006–0.076 μmol/m^2/d DFe from benthic provenance could be excreted by krill in the upper 200 m. If compared with our flux estimates in Table 4, this is a small flux in nearshore waters, but in deeper waters further offshore could become significant.

[55] A hitherto largely overlooked recycling pathway of Fe in the upper waters of the Southern Ocean could be via large animals, such as whales, seals, penguins and other sea birds. For instance, *Nicol et al.* [2010] estimated that whales convert annually 7600 tonnes of Fe associated with krill biomass into easily dispersible faecal slurry. Considering that the Antarctic krill has a distribution range of 19.10^6 km^2 [*Nicol et al.*, 2010] and assuming that whales reside 6 months in Antarctic waters, this would represent a recycling flux of 0.039 μmol/m^2/d of DFe and particulate Fe. How much of this is bioavailable has yet to be determined.

5.6. Residence Times of DFe

[56] To arrive at realistic modeled DFe concentrations in the Southern Ocean, *Moore and Braucher* [2008] required a global scavenging residence time of 0.65 year for an upper mixed layer of 103 m. If we assume steady state, so that the loss of DFe by scavenging on particles and subsequent sedimentation out of the upper mixed layer is balanced by DFe inputs, than the residence time as defined by upper mixed layer DFe inventory divided by DFe input should be of the same order if the DFe inputs that we estimated here were realistic. Using the annual fluxes from Table 5, we found residence times averaging at 0.82 ± 0.58 year, indeed suggesting that our flux estimates are realistic. The residence time also suggests that there is sufficient time for the shelf DFe input to be transported within the ACC more than 1500 km away. A still shorter residence time, i.e., a stronger scavenging rate, would mean that to maintain the observed DFe inventory in the upper mixed layer the fluxes need to be larger. On the one hand this would be limited to what sediments could produce in terms of new DFe, while on the other hand larger fluxes would mean that there would no longer be iron limitation in the Southern Ocean.

6. Conclusion

[57] Vertical profiles of DFe, PL-Fe and REF-Fe at two stations in the western Weddell Sea and the Weddell-Scotia Confluence demonstrate the role of the sediments in enriching the water column close to the Antarctic continent and potentially fertilizing coastal and open ocean waters. A compilation of these and other here newly presented DFe data as well as literature data from the Atlantic sector of the Southern Ocean, averaged over the upper 200 m, reveals an exponential eastward decrease as a function of distance from the nearest Antarctic Peninsula, South Sandwich Islands or western Weddell Sea shorelines. This decrease can be followed more than 3000 km away from the Antarctic Peninsula downstream the ACC. The associated lateral flux that we have attempted to calculate breaks down in a horizontal advection and a horizontal diffusive flux. They contribute 54 ± 15% and 1 ± 2% of the total summertime flux to the upper mixed layer (= horizontal advection + vertical advection + horizontal diffusion+ vertical diffusion + atmospheric fluxes). Vertical advection is an important DFe source also, with a contribution of 29 ± 13%. Atmospheric and vertical diffusive inputs are comparatively small with 15 ± 10% and 1 ± 1%, respectively. However, the assumptions regarding upwelling velocity, and average zonal velocity have large inherent uncertainties. This means that the relative importance of the horizontal and vertical advective fluxes could be more variable in time and space than suggested here. In any case, the lateral flux is the most important long-distance supplier of DFe to the Fe limited waters of the Atlantic sector of the Southern Ocean, and could be one of the driving forces behind the observed large-scale Chl *a* distributions downstream of the Antarctic Peninsula and the tip of the South American continent.

[58] Wintertime deep mixing appears to be an important mechanism to replenish DFe depleted surface waters in time for the next spring bloom. This represents 34 ± 21% of the annual new DFe supply to the upper mixed layer (= horizontal advection + horizontal diffusion+ winter mixing + atmospheric fluxes). Winter mixing could be a major contributor to the DFe inventory of sea ice through scavenging of upwelled DFe during its formation.

[59] During the spring sea ice melt in the marginal ice zone, the DFe supply could be increased by a factor of up to ten on a regional scale, thus creating the Fe replete circumstances necessary to support widespread ice edge blooms. Similarly, but probably on a more local scale, limited to areas where icebergs are present, melting icebergs could give rise to Fe replete conditions temporarily as well [*Lancelot et al.*, 2009].

[60] The observed carbon fixation by primary producers allowed us to estimate Fe fixation and to compare this with the DFe supply, for the open ocean and for continental shelf waters. This shows a twofold excess of new DFe input on the continental shelf and a one third shortage of new DFe input in the open ocean, assuming that all new DFe is bioavailable. The observed open ocean primary productivity in

the Atlantic sector of the Southern Ocean can only be sustained by recycling of Fe, with a "*fe*" of 0.59.

[61] **Acknowledgments.** We thank the captains and crews on several RV *Polarstern* expeditions for skillfully carrying out their tasks. We are indebted to the Alfred-Wegener-Institut für Polar- und Meeresforschung (AWI), Bremerhaven, Germany, for hosting us on its ship. Mike Schröder (AWI) and his team are thanked for carrying out the CTD operations during ISPOL. The Royal Belgian Institute of Natural Sciences is thanked for providing us with a clean air laboratory container during the ISPOL cruise. This study would not have been possible without the financial support from the ARC-SIBCLIM project (contract ARC-2/07-287) funded by the Belgian French Community, as well as the BELCANTO (contract SD/CA/03A) and BIGSOUTH (contract SD/CA/05A) projects funded by the Belgian Federal Science Policy Office. We are also grateful to the Fonds de la Recherche Scientifique (F.R.S.-FNRS, Belgium) for support of the MC-ICP-MS facility at ULB under FRFC contract 2.4617.06. We also acknowledge financial support under contract 851.20.046 from the Netherlands Polar Program of the Netherlands Organization for Scientific Research (NWO). The great scrutiny and detailed comments by two anonymous reviewers greatly improved the manuscript.

References

Absy, J. M., M. Schröder, R. D. Muench, and H. Hellmer (2008), Physical oceanography from 120 CTD stations during POLARSTERN cruise ANT-XXII/2(ISPOL), http://doi.pangaea.de/10.1594/PANGAEA.742627, PANGAEA, Network for Geol. and Environ. Data, Bremerhaven, Germany.

Aguilar-Islas, A. M., R. D. Rember, C. W. Mordy, and J. Wu (2008), Sea ice-derived dissolved iron and its potential influence on the spring algal bloom in the Bering Sea, *Geophys. Res. Lett.*, *35*, L24601, doi:10.1029/2008GL035736.

Ardelan, M. V., O. Holm-Hansen, C. D. Hewes, C. S. Reiss, N. S. Silva, H. Dulaiova, E. Steinnes, and E. Sakshaug (2010), Natural iron enrichment around the Antarctic Peninsula in the Southern Ocean, *Biogeosciences*, *7*, 11–25, doi:10.5194/bg-7-11-2010.

Arrigo, K. R., G. L. van Dijken, and S. Bushinsky (2008), Primary production in the Southern Ocean, 1997–2006, *J. Geophys. Res.*, *113*, C08004, doi:10.1029/2007JC004551.

Baker, A. R., T. D. Jickells, M. Witt, and K. L. Linge (2006), Trends in the solubility of iron, aluminum, manganese and phosphorus in aerosol collected over the Atlantic Ocean, *Mar. Chem.*, *98*, 43–58, doi:10.1016/j.marchem.2005.06.004.

Banse, K. (1996), Low seasonality of low concentrations of surface chlorophyll in the subantarctic water ring: Underwater irradiance, iron, or grazing?, *Prog. Oceanogr.*, *37*, 241–291, doi:10.1016/S0079-6611(96)00006-7.

Barbeau, K., J. W. Moffett, D. A. Caron, P. L. Croot, and D. L. Erdner (1996), Role of protozoan grazing in relieving iron limitation of phytoplankton, *Nature*, *380*, 61–64, doi:10.1038/380061a0.

Berger, C. J. M., S. M. Lippiatt, M. G. Lawrence, and K. W. Bruland (2008), Application of a chemical leach technique for estimating labile particulate aluminum, iron, and manganese in the Columbia River plume and coastal waters off Oregon and Washington, *J. Geophys. Res.*, *113*, C00B01, doi:10.1029/2007JC004703.

Best, S. E., V. O. Ivchenko, K. J. Richards, R. D. Smith, and R. C. Malone (1999), Eddies in numerical models of the Antarctic Circumpolar Current and their influence on the mean flow, *J. Phys. Oceanogr.*, *29*, 328–350, doi:10.1175/1520-0485(1999)029<0328:EINMOT>2.0.CO;2.

Blain, S., et al. (2007), Effect of natural iron fertilization on carbon sequestration in the Southern Ocean, *Nature*, *446*, 1070–1074, doi:10.1038/nature05700.

Blain, S., G. Sarthou, and P. Laan (2008), Distribution of dissolved iron during the natural iron-fertilization experiment KEOPS (Kerguelen Plateau, Southern Ocean), *Deep Sea Res., Part II*, *55*, 594–605, doi:10.1016/j.dsr2.2007.12.028.

Bonnin, J., W. van Raaphorst, G.-J. Brummer, H. van Haren, and H. Malschaert (2002), Intense mid-slope resuspension of particulate matter in the Faeroe–Shetland Channel: Short-term deployment of near-bottom sediment traps, *Deep Sea Res., Part I*, *49*, 1485–1505, doi:10.1016/S0967-0637(02)00030-4.

Bowie, A. R., M. T. Maldonado, R. C. Frew, P. L. Croot, E. P. Achterberg, R. F. C. Mantoura, P. J. Worsfold, C. S. Law, and P. W. Boyd (2001), The fate of added iron during a mesoscale fertilisation experiment in the Polar Southern Ocean, *Deep Sea Res., Part II*, *48*, 2703–2743, doi:10.1016/S0967-0645(01)00015-7.

Bowie, A. R., D. J. Whitworth, E. P. Achterberg, R. F. C. Mantoura, and P. J. Worsfold (2002), Biogeochemistry of Fe and other trace elements (Al, Co, Ni) in the upper Atlantic Ocean, *Deep Sea Res., Part I*, *49*, 605–636, doi:10.1016/S0967-0637(01)00061-9.

Bowie, A. R., D. Lannuzel, T. A. Remenyi, T. Wagener, P. J. Lam, P. W. Boyd, C. Guieu, A. T. Townsend, and T. W. Trull (2009), Biogeochemical iron budgets of the Southern Ocean south of Australia: Decoupling of iron and nutrient cycles in the subantarctic zone by the summertime supply, *Global Biogeochem. Cycles*, *23*, GB4034, doi:10.1029/2009GB003500.

Boyd, P. W., and M. J. Ellwood (2010), The biogeochemical cycle of iron in the ocean, *Nat. Geosci.*, *3*, 675–682, doi:10.1038/ngeo964.

Boyd, P. W., et al. (2005), FeCycle: Attempting an iron biogeochemical budget from a mesoscale SF_6 tracer experiment in unperturbed low iron waters, *Global Biogeochem. Cycles*, *19*, GB4S20, doi:10.1029/2005GB002494.

Boyd, P. W., et al. (2007), Mesoscale iron enrichment experiments 1993–2005: Synthesis and future directions, *Science*, *315*, 612–617, doi:10.1126/science.1131669.

Boyé, M., C. M. G. van den Berg, J. T. M. de Jong, H. Leach, P. Croot, and H. J. W. de Baar (2001), Organic complexation of iron in the Southern Ocean, *Deep Sea Res., Part I*, *48*, 1477–1497, doi:10.1016/S0967-0637(00)00099-6.

Bracher, A. U., B. M. A. Kroon, and M. I. Lucas (1999), Primary production, physiological state and composition of phytoplankton in the Atlantic sector of the Southern Ocean, *Mar. Ecol. Prog. Ser.*, *190*, 1–16, doi:10.3354/meps190001.

Bruland, K. W., E. L. Rue, and G. J. Smith (2001), Iron and macronutrients in California coastal upwelling regimes: Implications for diatom blooms, *Limnol. Oceanogr.*, *46*(7), 1661–1674, doi:10.4319/lo.2001.46.7.1661.

Bucciarelli, E., S. Blain, and P. Tréguer (2001), Iron and manganese in the wake of the Kerguelen Islands (Southern Ocean), *Mar. Chem.*, *73*, 21–36, doi:10.1016/S0304-4203(00)00070-0.

Carbotte, S. M., W. B. F. Ryan, S. O'Hara, R. Arko, A. Goodwillie, A. Melkonian, R. A. Weissel, and V. L. Ferrini (2007), Antarctic multibeam bathymetry and geophysical data synthesis: An on-line digital data resource for marine geoscience research in the Southern Ocean, *U.S. Geol. Surv. Open File Rep.*, *2007-1047*, 4 pp., doi:10.3133/of2007-1047.srp002.

Charette, M. A., M. E. Gonneea, P. J. Morris, P. Statham, G. Fones, H. Planquette, I. Salter, and A. Naveira Garabato (2007), Radium isotopes as tracers of iron sources fueling a Southern Ocean phytoplankton bloom, *Deep Sea Res., Part II*, *54*, 1989–1998, doi:10.1016/j.dsr2.2007.06.003.

Chase, Z., K. S. Johnson, V. A. Elrod, J. N. Plant, S. E. Fitzwater, L. Pickell, and C. M. Sakamoto (2005), Manganese and iron distributions off central California influenced by upwelling and shelf width, *Mar. Chem.*, *95*, 235–254, doi:10.1016/j.marchem.2004.09.006.

Chever, F., G. Sarthou, E. Bucciarelli, S. Blain, and A. R. Bowie (2010), An iron budget during the natural iron fertilisation experiment KEOPS (Kerguelen Islands, Southern Ocean), *Biogeosciences*, *7*, 455–468, doi:10.5194/bg-7-455-2010.

Coombs, D. S., and C. A. Landis (1966), Pumice from the South Sandwich eruption of March 1962 reaches New Zealand, *Nature*, *209*, 289–290, doi:10.1038/209289b0.

Croot, P. L., K. Andersson, M. Öztürk, and D. R. Turner (2004), The distribution and speciation of iron along 6°E in the Southern Ocean, *Deep Sea Res., Part II*, *51*, 2857–2879, doi:10.1016/j.dsr2.2003.10.012.

de Baar, H. J. W., J. T. M. de Jong, D. C. E. Bakker, B. M. Löscher, C. Veth, U. Bathmann, and V. Smetacek (1995), Importance of iron for plankton blooms and carbon dioxide drawdown in the Southern Ocean, *Nature*, *373*, 412–415, doi:10.1038/373412a0.

de Baar, H. J. W., J. T. M. de Jong, R. F. Nolting, K. R. Timmermans, M. A. van Leeuwe, U. Bathmann, M. Rutgers van der Loeff, and J. Sildam (1999), Low dissolved Fe and the absence of diatom blooms in remote Pacific waters of the Southern Ocean, *Mar. Chem.*, *66*, 1–34, doi:10.1016/S0304-4203(99)00022-5.

de Baar, H. J. W., L. J. A. Gerringa, P. Laan, and K. R. Timmermans (2008), Efficiency of carbon removal per added iron in ocean iron fertilization, *Mar. Ecol. Prog. Ser.*, *364*, 269–282, doi:10.3354/meps07548.

de Jong, J. T. M., J. den Das, U. Bathmann, M. H. C. Stoll, G. Kattner, R. F. Nolting, and H. J. W. de Baar (1998), Dissolved iron at subnanomolar levels in the Southern Ocean as determined by ship-board analysis, *Anal. Chim. Acta*, *377*, 113–124, doi:10.1016/S0003-2670(98)00427-9.

de Jong, J. T. M., M. Boyé, M. D. Gelado-Caballero, K. R. Timmermans, M. J. W. Veldhuis, R. F. Nolting, C. M. G. van den Berg, and H. J. W. de Baar (2007), Input of iron, aluminum and manganese to the surface mixed layer of the Northeast Atlantic Ocean and European continental shelf waters, *Mar. Chem.*, *107*, 120–142, doi:10.1016/j.marchem.2007.05.007.

de Jong, J., V. Schoemann, D. Lannuzel, J.-L. Tison, and N. Mattielli (2008), High-accuracy determination of iron in seawater by isotope

dilution multiple collector inductively coupled plasma mass spectrometry (ID-MC-ICP-MS) using nitrilotriacetic acid chelating resin for preconcentration and matrix separation, *Anal. Chim. Acta*, *623*, 126–139, doi:10.1016/j.aca.2008.06.013.

de Jonge, V. N., and J. E. E. van Beusekom (1995), Wind- and tide-induced resuspension of sediment and microphytobenthos from tidal flats in the Ems estuary, *Limnol. Oceanogr.*, *40*(4), 776–778, doi:10.4319/lo.1995.40.4.0776.

Dulaiova, H., M. V. Ardelan, P. B. Henderson, and M. A. Charette (2009), Shelf-derived iron inputs drive biological productivity in the southern Drake Passage, *Global Biogeochem. Cycles*, *23*, GB4014, doi:10.1029/2008GB003406.

Dumont, I., V. Schoemann, D. Lannuzel, L. Chou, J.-L. Tison, and S. Becquevort (2009), Distribution and characterization of dissolved and particulate organic matter in Antarctic pack ice, *Polar Biol.*, *32*, 733–750, doi:10.1007/s00300-008-0577-y.

Edwards, R., and P. Sedwick (2001), Iron in East Antarctic snow: Implications for atmospheric iron deposition and algal production in Antarctic waters, *Geophys. Res. Lett.*, *28*, 3907–3910, doi:10.1029/2001GL012867.

Edwards, R., P. Sedwick, V. Morgan, and C. Boutron (2006), Iron in ice cores from Law Dome: A record of atmospheric iron deposition for maritime East Antarctica during the Holocene and Last Glacial Maximum, *Geochem. Geophys. Geosyst.*, *7*, Q12Q01, doi:10.1029/2006GC001307.

Elrod, V. A., W. M. Berelson, K. H. Coale, and K. S. Johnson (2004), The flux of iron from continental shelf sediments: A missing source for global budgets, *Geophys. Res. Lett.*, *31*, L12307, doi:10.1029/2004GL020216.

Epping, E. H. G., V. Schoemann, and H. de Heij (1998), Manganese and iron oxidation during benthic oxygenic photosynthesis, *Estuarine Coastal Shelf Sci.*, *47*, 753–767, doi:10.1006/ecss.1998.0401.

Froneman, P. W., E. A. Pakhomov, and M. G. Balarin (2004), Size-fractionated phytoplankton biomass, production and biogenic carbon flux in the eastern Atlantic sector of the Southern Ocean in late austral summer 1997–1998, *Deep Sea Res., Part II*, *51*, 2715–2729, doi:10.1016/j.dsr2.2002.09.001.

Gaiero, D. M., J.-L. Probst, P. J. Depetris, S. M. Bidart, and L. Leleyter (2003), Iron and other transition metals in Patagonian riverborne and windborne materials: Geochemical control and transport to the southern South Atlantic Ocean, *Geochim. Cosmochim. Acta*, *67*, 3603–3623, doi:10.1016/S0016-7037(03)00211-4.

Garcia, V. M. T., C. A. E. Garcia, M. M. Mata, R. C. Pollery, A. R. Piola, S. R. Signorini, C. R. McClain, and M. D. Iglesias-Rodriguez (2008), Environmental factors controlling the phytoplankton blooms at the Patagonia shelf-break in spring, *Deep Sea Res., Part I*, *55*, 1150–1166, doi:10.1016/j.dsr.2008.04.011.

Gargett, A. E. (1984), Vertical eddy diffusivity in the ocean interior, *J. Mar. Syst.*, *42*, 359–393.

Gargett, A., J. Wells, A. E. Tejada-Martınez, and C. E. Grosch (2004), Langmuir supercells: A mechanism for sediment resuspension and transport in shallow seas, *Science*, *306*, 1925–1928, doi:10.1126/science.1100849.

Garrity, C. (2000), Real-time satellite information, *Ber. Polarforsch.*, *364*, 119–125.

Gassó, S., and A. F. Stein (2007), Does dust from Patagonia reach the sub-Antarctic Atlantic Ocean?, *Geophys. Res. Lett.*, *34*, L01801, doi:10.1029/2006GL027693.

Geibert, W., M. M. Rutgers van der Loeff, C. Hanfland, and H.-J. Dauelsberg (2002), Actinium-227 as a deep-sea tracer: Sources, distribution and applications, *Earth Planet. Sci. Lett.*, *198*, 147–165, doi:10.1016/S0012-821X(02)00512-5.

Gerringa, L. J. A., S. Blain, P. Laan, G. Sarthou, M. J. W. Veldhuis, C. P. D. Brussaard, E. Viollier, and K. R. Timmermans (2008), Fe-binding dissolved organic ligands near the Kerguelen Archipelago in the Southern Ocean (Indian sector), *Deep Sea Res., Part II*, *55*, 606–621, doi:10.1016/j.dsr2.2007.12.007.

Glover, D. M., W. J. Jenkins, and S. C. Doney (2011), *Modeling Methods for Marine Science*, 592 pp., Cambridge Univ. Press, Cambridge, U. K.

Hassler, C., and V. Schoemann (2009), Bioavailability of organically bound Fe to model phytoplankton of the Southern Ocean, *Biogeosciences*, *6*, 2281–2296, doi:10.5194/bg-6-2281-2009.

Hassler, C. S., V. Schoemann, C. Mancuso Nichols, E. C. V. Butler, and P. W. Boyd (2011), Saccharides enhance iron bioavailability to Southern Ocean phytoplankton, *Proc. Natl. Acad. Sci. U. S. A.*, *108*(3), 1076–1081, doi:10.1073/pnas.1010963108.

Heywood, K. J., A. C. Naveira Garabato, and D. P. Stevens (2002), High mixing rates in the abyssal Southern Ocean, *Nature*, *415*, 1011–1014, doi:10.1038/4151011a.

Hoffmann, L. J., I. Peeken, and K. Lochte (2008), Iron, silicate, and light co-limitation of three Southern Ocean diatom species, *Polar Biol.*, *31*(9), 1067–1080, doi:10.1007/s00300-008-0448-6.

Hofmann, E. (1985), The large-scale horizontal structure of the Antarctic Circumpolar Current from FGGE drifters, *J. Geophys. Res.*, *90*, 7087–7097, doi:10.1029/JC090iC04p07087.

Hopkinson, B. M., B. G. Mitchell, R. A. Reynolds, H. Wang, K. E. Selph, C. I. Measures, C. D. Hewes, O. Holm-Hansen, and K. A. Barbeau (2007), Iron limitation across chlorophyll gradients in the southern Drake Passage: Phytoplankton responses to iron addition and photosynthetic indicators of iron stress, *Limnol. Oceanogr.*, *52*(6), 2540–2554, doi:10.4319/lo.2007.52.6.2540.

Hosegood, P., J. Bonnin, and H. van Haren (2004), Solibore-induced sediment resuspension in the Faeroe-Shetland Channel, *Geophys. Res. Lett.*, *31*, L09301, doi:10.1029/2004GL019544.

Ito, T., P. Parekh, S. Dutkiewicz, and M. J. Follows (2005), The Antarctic circumpolar productivity belt, *Geophys. Res. Lett.*, *32*, L13604, doi:10.1029/2005GL023021.

Jickells, T. D. (1999), The inputs of dust derived elements to the Sargasso Sea: A synthesis, *Mar. Chem.*, *68*, 5–14, doi:10.1016/S0304-4203(99)00061-4.

Jochem, F. J., S. Mathot, and B. Quéguiner (1995), Size-fractionated primary production in the open Southern Ocean in austral spring, *Polar Biol.*, *15*, 381–392, doi:10.1007/BF00239714.

Johnson, K. S. (2001), Iron supply and demand in the upper ocean: Is extraterrestrial dust an important source of bioavailable iron?, *Global Biogeochem. Cycles*, *15*, 61–63, doi:10.1029/2000GB001295.

Johnson, K. S., R. M. Gordon, and K. H. Coale (1997), What controls dissolved iron concentrations in the world ocean?, *Mar. Chem.*, *57*, 137–161, doi:10.1016/S0304-4203(97)00043-1.

Johnson, K. S., F. P. Chavez, and G. E. Friederich (1999), Continental-shelf sediment as a primary source of iron for coastal phytoplankton, *Nature*, *398*, 697–700, doi:10.1038/19511.

Johnson, K. S., et al. (2007), Developing standards for dissolved iron in seawater, *Eos Trans. AGU*, *88*(11), 131, doi:10.1029/2007EO110003.

Kahru, M., B. G. Mitchell, S. T. Gille, C. D. Hewes, and O. Holm-Hansen (2007), Eddies enhance biological production in the Weddell-Scotia Confluence of the Southern Ocean, *Geophys. Res. Lett.*, *34*, L14603, doi:10.1029/2007GL030430.

Klinkhammer, G. P., C. S. Chin, R. A. Keller, A. Dahlmann, H. Sahling, G. Sarthou, S. Petersen, F. Smith, and C. Wilson (2001), Discovery of hydrothermal vent sites in Bransfield Strait, Antarctica, *Earth Planet. Sci. Lett.*, *193*, 395–407, doi:10.1016/S0012-821X(01)00536-2.

Klunder, M. B., P. Laan, R. Middag, H. J. W. de Baar, and J. van Ooijen (2011), Dissolved iron in the Southern Ocean (Atlantic sector), *Deep Sea Res., Part II*, *58*, 2678–2694, doi:10.1016/j.dsr2.2010.10.042.

Korb, R. E., M. J. Whitehouse, and P. Ward (2004), SeaWiFS in the Southern Ocean: Spatial and temporal variability in phytoplankton biomass around South Georgia, *Deep Sea Res., Part II*, *51*, 99–116, doi:10.1016/j.dsr2.2003.04.002.

Korb, R. E., M. J. Whitehouse, S. E. Thorpe, and M. Gordon (2005), Primary production across the Scotia Sea in relation to the physico-chemical environment, *J. Mar. Syst.*, *57*, 231–249, doi:10.1016/j.jmarsys.2005.04.009.

Korb, R. E., M. J. Whitehouse, A. Atkinson, and S. E. Thorpe (2008), Magnitude and maintenance of the phytoplankton bloom at South Georgia: A naturally iron-replete environment, *Mar. Ecol. Prog. Ser.*, *368*, 75–91, doi:10.3354/meps07525.

Laës, A., S. Blain, P. Laan, S. J. Ussher, E. P. Achterberg, P. Tréguer, and H. J. W. de Baar (2007), Sources and transport of dissolved iron and manganese along the continental margin of the Bay of Biscay, *Biogeosciences*, *4*, 181–194, doi:10.5194/bg-4-181-2007.

Lam, P. J., and J. K. B. Bishop (2008), The continental margin is a key source of iron to the HNLC North Pacific Ocean, *Geophys. Res. Lett.*, *35*, L07608, doi:10.1029/2008GL033294.

Lam, P. J., J. K. B. Bishop, C. C. Henning, M. A. Marcus, G. A. Waychunas, and I. Y. Fung (2006), Wintertime phytoplankton bloom in the subarctic Pacific supported by continental margin iron, *Global Biogeochem. Cycles*, *20*, GB1006, doi:10.1029/2005GB002557.

Lancelot, C., A. de Montety, H. Goosse, S. Becquevort, V. Schoemann, B. Pasquer, and M. Vancoppenolle (2009), Spatial distribution of iron supply to phytoplankton in the Southern Ocean: A model study, *Biogeosciences*, *6*, 2861–2878, doi:10.5194/bg-6-2861-2009.

Landing, W. M., and K. W. Bruland (1987), The contrasting biogeochemistry of iron and manganese in the Pacific Ocean, *Geochim. Cosmochim. Acta*, *51*, 29–43, doi:10.1016/0016-7037(87)90004-4.

Landing, W. M., C. Haraldsson, and N. Paxeus (1986), Vinyl polymer agglomerate based transition metal cation-chelating ion-exchange resin containing the 8-hydroxyquinoline functional group, *Anal. Chem.*, *58*(14), 3031–3035, doi:10.1021/ac00127a029.

Lannuzel, D., V. Schoemann, J. de Jong, J.-L. Tison, and L. Chou (2007), Distribution and biogeochemical behaviour of iron in the East Antarctic sea ice, *Mar. Chem.*, *106*, 18–32, doi:10.1016/j.marchem.2006.06.010.

Lannuzel, D., V. Schoemann, J. de Jong, L. Chou, B. Delille, S. Becquevort, and J.-L. Tison (2008), Iron study during a time series in the western Weddell pack ice, *Mar. Chem.*, *108*, 85–95, doi:10.1016/j.marchem.2007.10.006.

Lannuzel, D., V. Schoemann, J. de Jong, B. Pasquer, P. van der Merwe, F. Masson, J.-L. Tison, and A. Bowie (2010), Distribution of dissolved iron in Antarctic sea ice: Spatial, seasonal, and inter-annual variability, *J. Geophys. Res.*, *115*, G03022, doi:10.1029/2009JG001031.

Latimer, J. C., and G. M. Filippelli (2007), Sedimentary iron records from the Cape Basin, *Deep Sea Res., Part II*, *54*, 2422–2431, doi:10.1016/j.dsr2.2007.07.022.

Law, C. S., E. R. Abraham, A. J. Watson, and M. I. Liddicoat (2003), Vertical eddy diffusion and nutrient supply to the surface mixed layer of the Antarctic Circumpolar Current, *J. Geophys. Res.*, *108*(C8), 3272, doi:10.1029/2002JC001604.

Ledwell, J. R., A. J. Watson, and C. S. Law (1998), Mixing of a tracer in the pycnocline, *J. Geophys. Res.*, *103*, 21,499–21,529, doi:10.1029/98JC01738.

Lin, H., S. Rauschenberg, C. R. Hexel, T. J. Shaw, and B. S. Twining (2011), Free-drifting icebergs as sources of iron to the Weddell Sea, *Deep Sea Res., Part II*, *58*, 1392–1406, doi:10.1016/j.dsr2.2010.11.020.

Lohan, M. C., A. M. Aguilar-Islas, R. P. Franks, and K. W. Bruland (2005), Determination of iron and copper in seawater at pH 1.7 with a new commercially available chelating resin, NTA Superflow, *Anal. Chim. Acta*, *530*, 121–129, doi:10.1016/j.aca.2004.09.005.

Löscher, B. M., H. J. W. de Baar, J. T. M. De Jong, C. Veth, and F. Dehairs (1997), The distribution of Fe in the Antarctic Circumpolar Current, *Deep Sea Res., Part II*, *44*, 143–187, doi:10.1016/S0967-0645(96)00101-4.

Marshall, J., E. Shuckburgh, H. Jones, and C. Hill (2006), Estimates and implications of surface eddy diffusivity in the Southern Ocean derived from tracer transport, *J. Phys. Oceanogr.*, *36*(9), 1806–1821, doi:10.1175/JPO2949.1.

Martin, J. H. (1990), Glacial-interglacial CO_2 change: The iron hypothesis, *Paleoceanography*, *5*, 1–13, doi:10.1029/PA005i001p00001.

Martin, J. H., R. M. Gordon, and S. E. Fitzwater (1990), Iron in Antarctic waters, *Nature*, *345*, 156–158, doi:10.1038/345156a0.

Mathot, S., J.-M. Dandois, and C. Lancelot (1992), Gross and net primary production in the Scotia-Weddell Sea sector of the Southern Ocean during spring 1988, *Polar Biol.*, *12*, 321–332, doi:10.1007/BF00238275.

McCave, I. N. (1986), Local and global aspects of the bottom nepheloid layers in the world ocean, *Neth. J. Sea Res.*, *20*, 167–181, doi:10.1016/0077-7579(86)90040-2.

McConnell, J. R., A. J. Aristarain, J. R. Banta, P. R. Edwards, and J. C. Simoes (2007), 20th-century doubling in dust archived in an Antarctic Peninsula ice core parallels climate change and desertification in South America, *Proc. Natl. Acad. Sci. U. S. A.*, *104*, 5743–5748, doi:10.1073/pnas.0607657104.

Measures, C. I., and S. Vink (2000), On the use of dissolved aluminum in surface waters to estimate dust deposition to the ocean, *Global Biogeochem. Cycles*, *14*, 317–327, doi:10.1029/1999GB001188.

Measures, C. I., and S. Vink (2001), Dissolved Fe in the upper waters of the Pacific sector of the Southern Ocean, *Deep Sea Res., Part II*, *48*, 3913–3941, doi:10.1016/S0967-0645(01)00074-1.

Middag, R., H. J. W. de Baar, P. Laan, P. H. Cai, and J. C. van Ooijen (2011), Dissolved manganese in the Atlantic sector of the Southern Ocean, *Deep Sea Res., Part II*, *58*, 2661–2677, doi:10.1016/j.dsr2.2010.10.043.

Moore, J. K., and O. Braucher (2008), Sedimentary and mineral dust sources of dissolved iron to the world ocean, *Biogeosciences*, *5*, 631–656, doi:10.5194/bg-5-631-2008.

Naveira Garabato, A. C., E. L. McDonagh, D. P. Stevens, K. J. Heywood, and R. J. Sanders (2002), On the export of Antarctic Bottom Water from the Weddell Sea, *Deep Sea Res., Part II*, *49*, 4715–4742, doi:10.1016/S0967-0645(02)00156-X.

Naveira Garabato, A. C., K. L. Polzin, B. A. King, K. J. Heywood, and M. Visbeck (2004), Widespread intense turbulent mixing in the Southern Ocean, *Science*, *303*, 210–213, doi:10.1126/science.1090929.

Nédélec, F., P. J. Statham, and M. Mowlem (2007), Processes influencing dissolved iron distributions below the surface at the Atlantic Ocean–Celtic Sea shelf edge, *Mar. Chem.*, *104*, 156–170, doi:10.1016/j.marchem.2006.10.011.

Nicol, S., A. Bowie, S. Jarman, D. Lannuzel, K. M. Meiners, and P. van der Merwe (2010), Southern Ocean iron fertilization by baleen whales and Antarctic krill, *Fish Fish.*, *11*, 203–209, doi:10.1111/j.1467-2979.2010.00356.x.

Nishioka, J., S. Takeda, H. J. W. de Baar, P. L. Croot, M. Boye, P. Laan, and K. R. Timmermans (2005), Changes in the concentration of iron in different size fractions during an iron enrichment experiment in the open Southern Ocean, *Mar. Chem.*, *95*, 51–63, doi:10.1016/j.marchem.2004.06.040.

Nishioka, J., T. Ono, H. Saito, K. Sakaoka, and T. Yoshimura (2011), Oceanic iron supply mechanisms which support the spring diatom bloom in the Oyashio region, western subarctic Pacific, *J. Geophys. Res.*, *116*, C02021, doi:10.1029/2010JC006321.

Nodwell, L. M., and N. Price (2001), Direct use of inorganic colloidal iron by marine mixotrophic phytoplankton, *Limnol. Oceanogr.*, *46*(4), 765–777, doi:10.4319/lo.2001.46.4.0765.

Nolting, R. F., H. J. W. de Baar, A. J. van Bennekom, and A. Masson (1991), Cadmium, copper and iron in the Scotia Sea, Weddell Sea and Weddell/Scotia Confluence (Antarctica), *Mar. Chem.*, *35*, 219–243, doi:10.1016/S0304-4203(09)90019-6.

Obata, H., H. Karatani, and E. Nakayama (1993), Automated determination of iron in seawater by chelating resin concentration and chemiluminescence detection, *Anal. Chem.*, *65*, 1524–1528, doi:10.1021/ac00059a007.

Okubo, A. (1971), Oceanic diffusion diagrams, *Deep Sea Res. Oceanogr. Abstr.*, *18*, 789–802.

Orsi, A. H., W. D. Nowlin Jr., and T. Whitworth III (1993), On the circulation and stratification of the Weddell Gyre, *Deep Sea Res., Part I*, *40*, 169–203, doi:10.1016/0967-0637(93)90060-G.

Orsi, A. H., T. Whitworth III, and W. D. Nowlin Jr. (1995), On the meridional extent and fronts of the Antarctic Circumpolar Current, *Deep Sea Res., Part I*, *42*, 641–673, doi:10.1016/0967-0637(95)00021-W.

Pakhomova, S. V., P. O. J. Hall, M. I. Kononets, A. G. Rozanov, A. Tengberg, and A. V. Vershinin (2007), Fluxes of iron and manganese across the sediment–water interface under various redox conditions, *Mar. Chem.*, *107*, 319–331, doi:10.1016/j.marchem.2007.06.001.

Patterson, S. L., and H. A. Sievert (1980), The Weddell-Scotia Confluence, *J. Phys. Oceanogr.*, *10*, 1584–1610, doi:10.1175/1520-0485(1980)010<1584:TWSC>2.0.CO;2.

Planquette, H., et al. (2007), Dissolved iron in the vicinity of the Crozet Islands, Southern Ocean, *Deep Sea Res., Part II*, *54*, 1999–2019, doi:10.1016/j.dsr2.2007.06.019.

Raiswell, R., L. G. Benning, M. Tranter, and S. Tulaczyk (2008), Bioavailable iron in the Southern Ocean: The significance of the iceberg conveyor belt, *Geochem. Trans.*, *9*(7), doi:10.1186/1467-4866-9-7.

Rey, J., L. Somoza, and J. Martinez-Frias (1995), Tectonic, volcanic, and hydrothermal event sequence on Deception Island (Antarctica), *Geo Mar. Lett.*, *15*, 1–8, doi:10.1007/BF01204491.

Ryan, W. B. F., et al. (2009), Global Multi-Resolution Topography (GMRT) synthesis data set, *Geochem. Geophys. Geosyst.*, *10*, Q03014, doi:10.1029/2008GC002332.

Riffenburgh, B. (2007), *Encyclopedia of the Antarctic*, 1408 pp., Routledge, New York.

Sachs, O., E. J. Sauter, M. Schlüter, M. M. Rutgers van der Loeff, K. Jerosch, and O. Holby (2009), Benthic organic carbon flux and oxygen penetration reflect different plankton provinces in the Southern Ocean, *Deep Sea Res., Part I*, *56*, 1319–1335, doi:10.1016/j.dsr.2009.02.003.

Sander, S. G., and A. Koschinsky (2011), Metal flux from hydrothermal vents increased by organic complexation, *Nat. Geosci.*, *4*, 145–150, doi:10.1038/ngeo1088.

Sañudo-Wilhelmy, S. A., K. A. Olsen, J. M. Scelfo, T. D. Foster, and A. R. Flegal (2002), Trace metal distributions off the Antarctic Peninsula in the Weddell Sea, *Mar. Chem.*, *77*, 157–170, doi:10.1016/S0304-4203(01)00084-6.

Sarthou, G., K. R. Timmermans, S. Blain, and P. Tréguer (2005), Growth physiology and fate of diatoms in the ocean: A review, *J. Sea Res.*, *53*, 25–42, doi:10.1016/j.seares.2004.01.007.

Sarthou, G., D. Vincent, U. Christaki, I. Obernosterer, K. R. Timmermans, and C. P. D. Brussaard (2008), The fate of biogenic iron during a phytoplankton bloom induced by natural fertilisation: Impact of copepod grazing, *Deep Sea Res., Part II*, *55*, 734–751, doi:10.1016/j.dsr2.2007.12.033.

Schmidt, K., et al. (2011), Seabed foraging by Antarctic krill: Implications for stock assessment, bentho-pelagic coupling, and the vertical transfer of iron, *Limnol. Oceanogr.*, *56*(4), 1411–1428, doi:10.4319/lo.2011.56.4.1411.

Schodlok, M. P., H. H. Hellmer, and A. Beckmann (2002), On the transport, variability and origin of dense water masses crossing the South Scotia Ridge, *Deep Sea Res., Part II*, *49*, 4807–4825, doi:10.1016/S0967-0645(02)00160-1.

Schoemann, V., H. J. W. de Baar, J. T. M. de Jong, and C. Lancelot (1998), Effects of phytoplankton blooms on the cycling of manganese and iron in coastal waters, *Limnol. Oceanogr.*, *43*(7), 1427–1441, doi:10.4319/lo.1998.43.7.1427.

Schwarz, J. N., and M. P. Schodlok (2009), Impact of drifting icebergs on surface phytoplankton biomass in the Southern Ocean: Ocean colour

remote sensing and in situ iceberg tracking, *Deep Sea Res., Part I*, *56*, 1727–1741, doi:10.1016/j.dsr.2009.05.003.

Severmann, S., J. McManus, W. M. Berelson, and D. E. Hammond (2010), The continental shelf benthic iron flux and its isotopic composition, *Geochim. Cosmochim. Acta*, *74*, 3984–4004, doi:10.1016/j.gca.2010.04.022.

Smetacek, V., H. J. W. de Baar, U. Bathmann, K. Lochte, and M. M. Rutgers van der Loeff (1997), Physical oceanography during POLARSTERN cruise ANT-X/6, http://doi.pangaea.de/10.1594/PANGAEA.759261, PANGAEA, Network for Geol. and Environ. Data, Bremerhaven, Germany.

Smetacek, V., C. Klaas, S. Menden-Deuer, and T. A. Rynearson (2002), Mesoscale distribution of dominant diatom species relative to the hydrographical field along the Antarctic Polar Front, *Deep Sea Res., Part II*, *49*, 3835–3848, doi:10.1016/S0967-0645(02)00113-3.

Smith, D. A., E. E. Hofmann, J. M. Klinck, and C. M. Lascara (1999), Hydrography and circulation of the West Antarctic Peninsula Continental Shelf, *Deep Sea Res., Part I*, *46*, 925–949, doi:10.1016/S0967-0637(98)00103-4.

Smith, K. L., Jr., B. H. Robison, J. J. Helly, R. S. Kaufmann, H. A. Ruhl, T. J. Shaw, B. S. Twining, and M. Vernet (2007), Free-drifting icebergs: Hot spots of chemical and biological enrichment in the Weddell Sea, *Science*, *317*, 478–482, doi:10.1126/science.1142834.

Statham, P. J., M. Skidmore, and M. Tranter (2008), Inputs of glacially derived dissolved and colloidal iron to the coastal ocean and implications for primary productivity, *Global Biogeochem. Cycles*, *22*, GB3013, doi:10.1029/2007GB003106.

Strass, V. (2010), Physical oceanography during POLARSTERN cruise ANT-XVI/3, http://doi.pangaea.de/10.1594/PANGAEA.742582, PANGAEA, Network for Geol. and Environ. Data, Bremerhaven, Germany.

Strass, V., and G. Rohardt (2010), Physical oceanography during POLARSTERN cruise ANT-XIII/2, http://doi.pangaea.de/10.1594/PANGAEA.735282, PANGAEA, Network for Geol. and Environ. Data, Bremerhaven, Germany.

Strzepek, R. F., M. T. Maldonado, J. L. Higgins, J. Hall, K. Safi, S. W. Wilhelm, and P. W. Boyd (2005), Spinning the "Ferrous Wheel": The importance of the microbial community in an iron budget during the FeCycle experiment, *Global Biogeochem. Cycles*, *19*, GB4S26, doi:10.1029/2005GB002490.

Sundermeyer, M. A., and J. F. Price (1998), Lateral mixing and the North Atlantic Tracer Release Experiment: Observations and numerical simulations of Lagrangian particles and a passive tracer, *J. Geophys. Res.*, *103*, 21,481–21,497, doi:10.1029/98JC01999.

Tagliabue, A., et al. (2010), Hydrothermal contribution to the oceanic dissolved iron inventory, *Nat. Geosci.*, *3*, 252–256, doi:10.1038/ngeo818.

Tovar-Sánchez, A., C. M. Duarte, S. Hernández-León, and S. A. Sañudo-Wilhelmy (2007), Krill as a central node for iron cycling in the Southern Ocean, *Geophys. Res. Lett.*, *34*, L11601, doi:10.1029/2006GL029096.

Tovar-Sánchez, A., C. M. Duarte, J. C. Alonso, S. Lacorte, R. Tauler, and C. Galbán-Malagón (2010), Impacts of metals and nutrients released from melting multiyear Arctic sea ice, *J. Geophys. Res.*, *115*, C07003, doi:10.1029/2009JC005685.

Twining, B. S., S. B. Baines, and N. S. Fisher (2004), Element stoichiometries of individual plankton cells collected during the Southern Ocean Iron Experiment (SOFeX), *Limnol. Oceanogr.*, *49*(6), 2115–2128, doi:10.4319/lo.2004.49.6.2115.

van der Merwe, P., D. Lannuzel, A. R. Bowie, C. A. Mancuso Nichols, and K. M. Meiners (2011), Iron fractionation in pack and fast ice in East Antarctica: Temporal decoupling between the release of dissolved and particulate iron during spring melt, *Deep Sea Res., Part II*, *58*, 1222–1236, doi:10.1016/j.dsr2.2010.10.036.

von Gyldenfeldt, A.-B., E. Fahrbach, M. A. Garcia, and M. Schröder (2002), Flow variability at the tip of the Antarctic Peninsula, *Deep Sea Res., Part II*, *49*, 4743–4766, doi:10.1016/S0967-0645(02)00157-1.

Wagener, T., C. Guieu, R. Losno, S. Bonnet, and N. Mahowald (2008), Revisiting atmospheric dust export to the Southern Hemisphere ocean: Biogeochemical implications, *Global Biogeochem. Cycles*, *22*, GB2006, doi:10.1029/2007GB002984.

Wedepohl, K. H. (1995), The composition of the continental crust, *Geochim. Cosmochim. Acta*, *59*, 1217–1232, doi:10.1016/0016-7037(95)00038-2.

Westerlund, S., and P. Öhman (1991), Iron in the water column of the Weddell Sea, *Mar. Chem.*, *35*, 199–217, doi:10.1016/S0304-4203(09)90018-4.

Whitworth, T., III, W. D. Nowlin Jr., A. H. Orsi, R. A. Locarnini, and S. G. Smith (1994), Weddell Sea Shelf Water in the Bransfield Strait and Weddell-Scotia Confluence, *Deep Sea Res., Part I*, *41*, 629–641, doi:10.1016/0967-0637(94)90046-9.

Yücel, M., A. Gartman, C. S. Chan, and G. W. Luther (2011), Hydrothermal vents as a kinetically stable source of iron-sulphide-bearing nanoparticles to the ocean, *Nat. Geosci.*, *4*, 367–371, doi:10.1038/ngeo1148.

P. Croot, Earth and Ocean Sciences, National University of Ireland, Galway, Quadrangle Building, University Road, Galway, Ireland.

H. de Baar, J. de Jong, and V. Schoemann, Department of Biological Oceanography, Royal Netherlands Institute for Sea Research, PO Box 59, NL-1790 AB, Texel, Netherlands.

D. Lannuzel, Institute for Marine and Antarctic Studies, University of Tasmania, Private Bag 129, Hobart, Tas 7005, Australia.

J.-L. Tison, Laboratoire de Glaciologie CP160/03, Département des Sciences de la Terre et de l'Environnement, Université Libre de Bruxelles, Ave. F. D. Roosevelt 50, B-1050, Brussels, Belgium.